Neutron Instruments for Research in Coordination Chemistry

Zi-Ling Xue,*[,1] Anibal J. Ramirez-Cuesta,*[,2] Craig M. Brown,[3,4] Stuart Calder,[2] Huibo Cao,[2] Bryan C. Chakoumakos,[2] Luke L. Daemen,[2] Ashfia Huq,[2] Alexander I. Kolesnikov,[2] Eugene Mamontov,[2] Andrey A. Podlesnyak,[2] and Xiaoping Wang[2]

[1] Prof. Zi-Ling Xue, *Department of Chemistry, University of Tennessee, Knoxville, Tennessee 37996, United States;* Email: xue@ion.chem.utk.edu; Web: https://xue.utk.edu/

[2] Dr. Anibal J. Ramirez-Cuesta, Dr. Stuart Calder, Dr. Huibo Cao, Dr. Bryan C. Chakoumakos, Dr. Luke L. Daemen, Dr. Ashfia Huq, Dr. Alexander I. Kolesnikov, Dr. Eugene Mamontov, Dr. Andrey A. Podlesnyak, and Dr. Xiaoping Wang, *Neutron Scattering Division, Oak Ridge National Laboratory, Oak Ridge, Tennessee 37831, United States*; Email: ramirezcueaj@ornl.gov; Web: https://neutrons.ornl.gov/contacts/ramirezcueaj

[3] Dr. Craig M. Brown, *Center for Neutron Research, National Institute of Standards and Technology, Gaithersburg, Maryland 20899, United States;* [4] *Department of Chemical and Biomolecular Engineering, University of Delaware, Newark, Delaware 19716, United States*

Abstract

Neutron diffraction and spectroscopies offer unique insight into structures and properties of solids and molecular materials. All neutron instruments located at the various neutron sources are distinct, even if their designs are based on similar principles, and thus, are usually less familiar to the community than commercial X-ray diffractometers and optical spectrometers. Major neutron instruments in the USA, which are open to scientists around the world, and examples of their use in coordination chemistry research are presented here, along with a list of

similar instruments at main neutron facilities in other countries. The reader may easily and quickly find from this mini-review an appropriate neutron instrument for research. The instruments include single-crystal and powder diffractometers to determine structures, inelastic neutron scattering (INS) spectrometers to probe magnetic and vibrational excitations, and quasielastic neutron scattering (QENS) spectrometers to study molecular dynamics such as methyl rotation on ligands. Key and unique features of the diffraction and neutron spectroscopies that are relevant to inorganic chemistry are reviewed.

Introduction

Neutron diffraction and spectroscopies have long been used in the studies of coordination chemistry, providing structures and revealing magnetic and other spectroscopic properties of complexes.[1] Neutron user facilities around the world provide instruments and resources to industrial, academic, and government entities to conduct the experiments. The Spallation Neutron Source (SNS)[2] at Oak Ridge National Laboratory (ORNL, Oak Ridge, Tennessee) in the US, the most intense pulsed neutron beams in the world for scientific research, has recently provided many new instruments. The instruments at SNS, plus those at High Flux Isotope Reactor (HFIR),[3] also at ORNL, and National Institute of Standards and Technology (NIST) Center for Neutron Research (NCNR, Gaithersburg, Maryland) in the US,[4] are user facilities open to scientists around the world to do neutron research.

Unique features of neutron scattering derive from the distinct wave-particle duality of the neutron, its zero charge, magnetic (spin) features, and the strength of interaction with the nucleus.[1c, d, 5] With no charge, neutrons penetrate deeply into a target and are scattered by nuclei

of atoms and unpaired electrons of the atoms. Atoms of different elements or isotopes (nuclides) of a particular element, with different combinations of protons and neutrons in the nuclei, have different nuclear forces that scatter (or absorb) incident neutrons. Thus, each isotope has a unique property to scatter neutrons known as the neutron scattering cross-section. In comparison, X-ray scattering is a result of scattering of photons from electrons with strong dependence on atomic number Z of the atom. The distinction becomes clear in the case of determining structure, where X-ray diffraction can give an electron density map of a single crystal. Neutron diffraction gives accurate positions of the nuclei. The H atoms in molecular systems are virtually transparent to X-rays but scatter neutrons strongly.[1c, 5a] Elements with similar atomic numbers Z, such as C and N or Mn and Fe, may be difficult to distinguish in X-ray diffraction but are easily distinguished by neutron diffraction. In addition, H and D isotopes scatter neutrons differently (mostly 'incoherent' and 'coherent', respectively), making it easier, for example, to distinguish H and D atoms in a molecule and emphasize spectroscopic or structural information content in the scattered neutron beam. In addition, neutron diffraction often provides more accurate bonding details, especially for atoms of light elements.

Neutrons may transfer some of their kinetic energies to samples through inelastic neutron scattering (INS), leading to magnetic and vibrational transitions.[1d] Neutrons carry spins and interact with unpaired electron spins in the sample, leading to magnetic transitions among low-lying energy levels[6] of as small as <1 cm^{-1}.[6g] Unlike IR and Raman spectroscopies which are subject to different rules of optical selection, INS for vibrations has no such rules and it gives a wide spectral range of 16-4,000 cm^{-1}.[1d] Thus, all vibrations are active in INS, and the spectra are particularly sensitive to H atom vibrations. These features make INS spectra readily and rigorously modeled, usually using *ab initio* methods, without the complications from electro-

optic parameters.

Each neutron instrument is specially designed with distinct features and trade-offs in design, function, and capabilities are often encountered. This mini-review summarizes key features of major neutron instruments relevant to coordination chemistry research, which should help the reader link the appropriate instruments to her/his research. Here, we provide first a brief overview of neutron generation and scatterings formalism for diffraction and spectroscopies. Key features of major neutron instruments in the USA are then discussed with examples of their use in coordination (and inorganic) chemistry research. Instruments at neutron facilities in other countries, mainly the ISIS Neutron and Muon Source (Chilton, UK), Institut Laue–Langevin (ILL, Grenoble, France), Heinz Maier-Leibnitz (FRM II, Munich, Germany), Helmholtz-Zentrum Berlin für Materialien und Energie (HZB, Berlin, Germany), Frank Laboratory of Neutron Physics (FLNP, Dubna, Russia), Paul Scherrer Institut (PSI, Villigen, Switzerland), and the Japan Proton Accelerator Research Complex (J-PARC, Tokai, Japan) are listed in the relevant sections to illustrate the capabilities around the globe.

1. Overview of Neutron Generation, Diffraction and Inelastic Neutron Scattering (INS)

There have been many publications on neutron diffraction and spectroscopies,[1a-d, 1f-j, 5, 7] including books on fundamental physics of neutron scattering by Furrer and coauthors[5b] and by Squires,[5a] an earlier book on neutron scattering in chemistry by Bacon[1a] and a more recent review on the subject by Pusztai,[1b] a book on single-crystal neutron diffraction by Wilson,[1c] and another book on vibrational spectroscopy with neutrons and its applications in chemistry (among others) by Mitchell and coauthors.[1d] An overview is given here of the generation of neutron beams, elastic neutron scattering for diffraction, and inelastic neutron scattering (INS)

and quasielastic neutron scattering (QENS) for spectroscopies.

1.1. Neutron Generation

A neutron beam is typically generated by one of the following two methods:[1d] (1) Fission of a radioactive nuclide such as U-235 in a reactor (known as *reactor sources*);[1d] (2) Spallation of a heavy metal target such as mercury,[2, 8] tungsten,[9] or lead[10] by a high-energy proton beam[11] (known as a spallation source).

U-235 fission is a more traditional method to generate neutrons. Neutrons are used to induce U-235 fission yielding yet more neutrons, a fraction of which after cooling (moderating) is sent to instruments as a continuous neutron beam with a broad energy distribution.[1d] Facilities that use the U-235 fission to make neutrons include the High Flux Isotope Reactor (HFIR) at ORNL,[3] Neutron-Beam Split Core Reactor (NBSR) reactor at NIST,[4] high-flux reactor at Institut Laue-Langevin (ILL, Grenoble, France),[12] FRM II (Munich, Germany),[13] Budapest Research Reactor (Budapest, Hungary),[14] and OPAL reactor at the Australian Centre for Neutron Scattering[15] (ANSTO, Lucas Heights, Australia). The IBR-2 reactor at the Joint Institute for Nuclear Research (Dubna, Russia), however, is an exception in that it uses fission of plutonium (in PuO_2) to generate neutrons.[1d, 16] In addition, two movable neutron reflectors at IBR-2 give a pulsed neutron beam in contrast to continuous neutron beam in other reactor-based neutron sources.[1d, 16]

Spallation process typically uses a pulsed, high-energy proton beam to collide with a target of heavy metal rich in neutrons. The protons excite the nuclei into a highly energetic state, evaporating nucleons (mostly neutrons) from the nuclei.[1d] Some of the neutrons spall off the target, giving, e.g., 60 pulses per second of neutrons at SNS.[1d] Other neutrons continue to trigger further reactions. In the process, each proton generates about 15-30 neutrons, yielding a

very intense neutron pulse. Unlike U-235 in the reactor sources, the target metal here is not required to be naturally fissile. Spallation sources include Spallation Neutron Source (SNS)[2] at ORNL, ISIS Neutron and Muon Source at Rutherford Appleton Laboratory (Chilton, UK),[1d, 11] J-PARC (Japan),[17] and the new China Spallation Neutron Source (CSNS) which has just started commissioning.[18] An exception to the pulsed spallation design is the Swiss Spallation Neutron Source (SINQ), a continuous source at Paul Scherrer Institut (PSI, Villigen, Switzerland).[1d, 19] SINQ could be considered to be a reactor source without the disadvantage of using fissile material such as U-235.[1d] In Sweden, European Spallation Source (ESS) is being constructed and the user program is expected to start in 2023.[20]

Newly generated neutrons usually have energies higher than needed for either diffraction or spectroscopies. Thus, their energies are reduced by passing the neutron beams through moderators of various types to produce neutrons of the desired wavelength (energy).[1b]

1.2. Neutron Scattering

When incident neutrons penetrate a sample, they are typically scattered due to interactions with either the nuclei of the atoms or unpaired electrons (spins). The scattering by unpaired electrons in a sample is called magnetic scattering, as it is the result of magnetic interactions between neutron spins and electron spins. Basic theories of both types of scattering have been discussed in detail elsewhere.[5] A qualitative description of the scattering processes is given here.

Some scattered neutrons have the same energy as the incident neutrons but simply change their direction. Such a scattering process is called elastic neutron scattering. Other neutrons undergo energy transfer with the sample during the scattering process. These neutrons not only

change their direction but also energy. Such a scattering process is called inelastic neutron scattering (INS). Both elastic and inelastic neutron scattering occur at the same time during interaction with the sample, and some neutron instruments are designed to measure both aspects simultaneously. For thermal neutrons, their wavelengths match the characteristic length scales of interatomic spacing in solids and their energies are in the same range of magnetic and vibrational excitations. As a consequence, the very same neutron can probe both structural and dynamical properties. This is not the case of photon scattering. For example, X-ray is required to study molecular structures by diffraction, while a laser (a different light source) is required to do Raman spectroscopy of the molecules. Diffraction from elastic scattering and spectroscopies from inelastic scattering are discussed below.

The elastic and inelastic scatterings may be represented using vectors in Scheme 1. The incident neutron has a wavelength λ_i and corresponding momentum $\boldsymbol{k_i}$ ($= 2\pi/\lambda_i$). The neutron is scattered by the sample, giving outgoing (final) neutron momentum $\boldsymbol{k_f}$ ($= 2\pi/\lambda_f$) (Scheme 1-Left) with a wavelength λ_f and the resulting vector of momentum transfer, $\boldsymbol{Q} = \boldsymbol{k_i} - \boldsymbol{k_f}$.

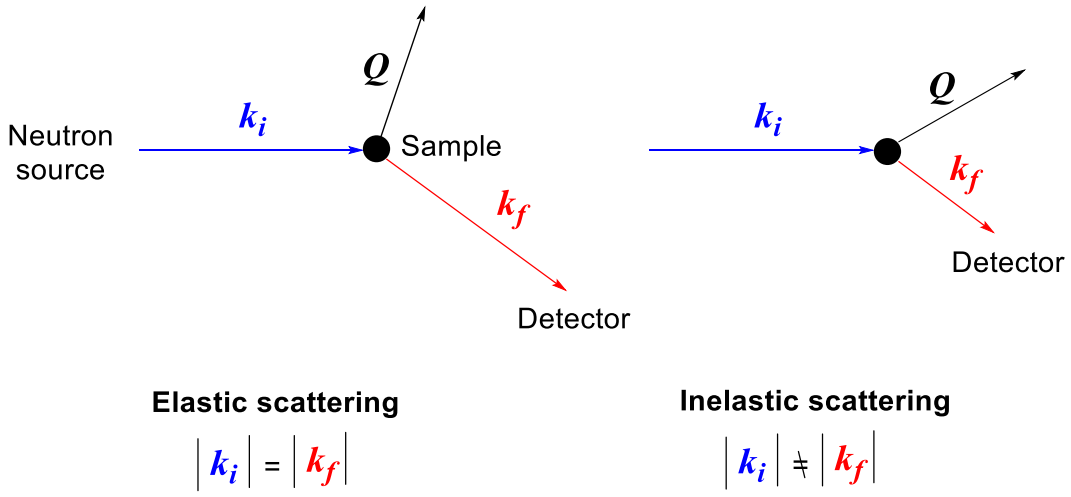

Scheme 1. Schematic of the neutron scattering processes. $\boldsymbol{k_i}$ and $\boldsymbol{k_f}$ refer to the momenta of the

incoming and outgoing neutrons, respectively. $\boldsymbol{Q} = \boldsymbol{k_i} - \boldsymbol{k_f}$ is the momentum transfer.

For neutrons from a reactor source, they are typically monochromated to a single wavelength or equivalently, energy. This is achieved in by either interaction with a monochromator,[1c] which is often composed of (somewhat imperfect) single crystals that diffract neutrons, or, using a series of choppers to select pulsed neutrons, before they reach the sample. For pulsed spallation sources, no monochromator is used in the diffraction measurements. Instead, the time-of-flight (TOF) technique is used to determine the energies of scattered neutrons based on the times they reach the detectors relative to when the pulse was started.[1c, 21] The advantage of the TOF diffraction technique is that a much more intense neutron beam (than in the reactor sources) can be used for diffraction, making data collection more efficient.

1.2.1. Diffraction

Neutron wavelengths can be modulated to the range of atomic distances in solid crystals. Thus, when neutrons collide with a crystalline sample, the elastic scattered neutrons from crystals may interfere, giving diffraction effects that follows the Bragg's law (Scheme 2).[1c] As in the case of X-ray diffraction, both powder and single-crystal samples may be used in neutron diffraction. Examples of both powder and single-crystal neutron diffraction to give structures of coordination complexes are given below. In addition, the book by Wilson offers more details of single-crystal neutron diffraction from molecular solids.[1c] In short, the structure information through neutron diffraction is from neutrons that undergo elastic scattering with the *nuclei* of the crystalline sample and later interfere to give rise to Bragg peaks. If single crystals can be grown, a structure solution is relatively straightforward and is the preferred method. Depending on the

crystal size and necessary *Q*-space coverage, this technique can be relatively slow, and not always suitable for parametric studies in which case powder diffraction may be suitable alternative. If there are no suitable crystals to solve a structure from, powder diffraction is the next best option for structure solution or structure refinement.

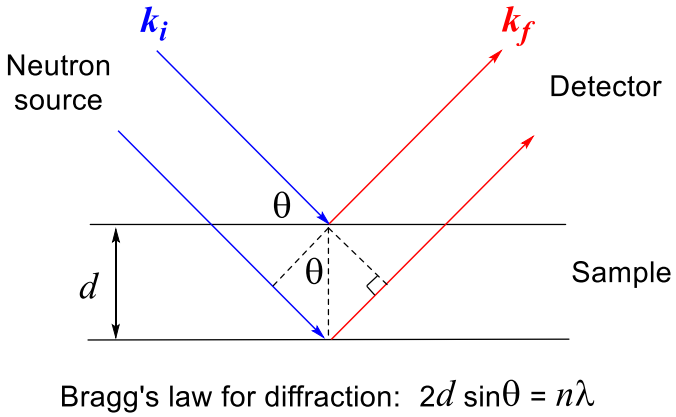

Scheme 2. Schematic of elastic neutron scattering process, leading to diffraction. $\boldsymbol{k_i}$ and $\boldsymbol{k_f}$ refer to the wavevectors of the incoming and outgoing neutrons, respectively.

When neutrons are scattered by unpaired electrons in a single crystal through the magnetic interactions and the scattered neutrons interfere, the diffraction provides spin density of the crystal.[7] For polarized neutron diffraction (PND), an instrument with polarization capabilities, such as a triple axis instrument with ^{3}He polarized gas cells, or a dedicated diffractometer such as D3 at ILL,[22] is used to measure the spin density. For D3, neutrons pass through a polarizing monochromator and then a spin flipper to give neutron beams with either up or down spins at the single crystal inside an external magnetic field. The unpaired electron spins of the crystals are aligned "up" with the magnetic field at, e.g., 2 K. The up- and down-spin neutrons have different interactions with the "up" electron spins, leading to different diffraction

intensities, which can be used to yield spin density of the crystal. One example of its use is the determination of spin density and which Fe(III) ions (S = 5/2) have up spins and which have down spins in $[Fe_8O_2(OH)_{12}(tacn)_6]Br_{4.3}(ClO_4)_{3.7}\cdot 6H_2O$ (Fe_8pcl; tacn = 1,4,7-triazacyclononane).[23] The two Fe(III) ions in blue color in Figure 1 carry down spins, and the other six Fe atoms in red color carry up spins.[7] Determination of spin density in chemical compounds, especially those with organic groups or ligands, is challenging at present, mainly because that the number of magnetic diffraction peaks from PND is often insufficient to give spin density.[7] The use of polarized neutron diffraction to give spin density has been reviewed.[7] Powder samples can also give rise to magnetic scattering and is often used to solve the magnetic structures of materials. Instrument descriptions and examples of results obtained for both single crystals and powder work are discussed in Section 2.

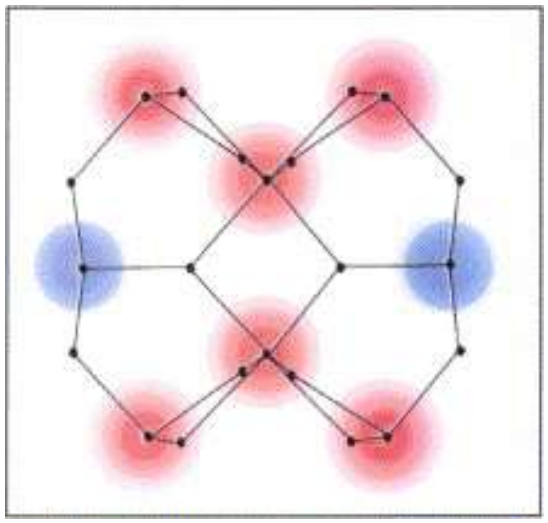

Figure 1. Magnetization density map in Fe_8pcl.[23] Reprinted with permission by Elsevier.

As indicated in the introduction, neutron scattering is an ideal tool to study the locations and vibrations of light elements, especially hydrogen. The most common isotope of hydrogen,

protium, has a very large incoherent scattering cross section. Protium and the other isotope of hydrogen, deuterium, have negative and positive scattering lengths of -3.74 and 6.67, respectively. The large incoherent scattering cross section leads to high background that is dependent on neutron energy and hence its wavelength. In addition, inelastic scattering cross section for 1-2 Å neutrons, which is often used for diffraction, can increase as a function of temperature and protium contents (or more commonly called hydrogen contents) of the samples. While the presence of hydrogen in the samples is not usually difficult to address in single-crystal diffraction (as discussed in the section on TOPAZ below), it is often more challenging in powder neutron diffraction. However, as shown in Figure 2, with very high flux available in current state-of-the-art powder diffractometers, large hydrogen atom percent samples are still feasible to study. Wilson et al. published an extensive review in 2014 on studying hydrogenous materials using neutron diffraction.[24]

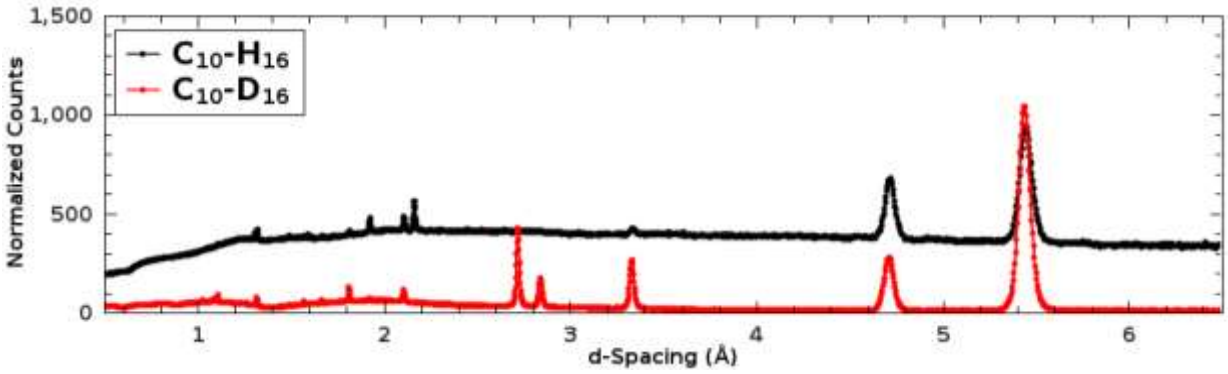

Figure 2. Diffraction pattern of protio- and deuterio-adamantane collected at POWGEN which is discussed below. The substantially large background in the hydrogenous sample appears due to the large incoherent scattering cross section of hydrogen which is missing in the deuterium-containing sample. The Bragg intensities differ due to the opposite sign of scattering length.

1.2.2. Spectroscopies from Inelastic Neutron Scattering (INS)

In INS processes at low temperature, the sample more likely gains energy from the neutron, leading to excitation from a lower energy state to a higher energy state. The sample may also lose energy, going from a higher energy to a lower energy state, leading to neutron energy gain. An example of using INS to probe magnetic transitions in [Mn(TPP)Cl] ($S = 2$; axial zero-field splitting parameter $D = -2.24(3)$ cm^{-1}; TPP^{2-} = tetraphenylporphyrinate) is given in Figure 3.[6g] At 2.1 K, only the ground $M_S = \pm 2$ is populated, giving only one large peak at 6.70(3) cm^{-1} = $3D$ for the transition to $M_S = \pm 1$. At 5.1 K, the $M_S = \pm 1$ state is populated and its transition $M_S = \pm 1 \rightarrow 0$ gives a second peak at 2.24(3) cm^{-1} = D. As the temperature is increased to 10.2 K and 50.0 K, the $M_S = \pm 1$ is more populated while the $M_S = \pm 2$ is depopulated, leading to the changes in the intensities of the two INS peaks. In addition, the "emission" peaks at -6.70(3) cm^{-1} and -2.24(3) cm^{-1} are also becoming more prominent as temperature increases, as they correspond to $M_S = 0 \rightarrow \pm 1$ and $\pm 1 \rightarrow \pm 2$ transitions, respectively.

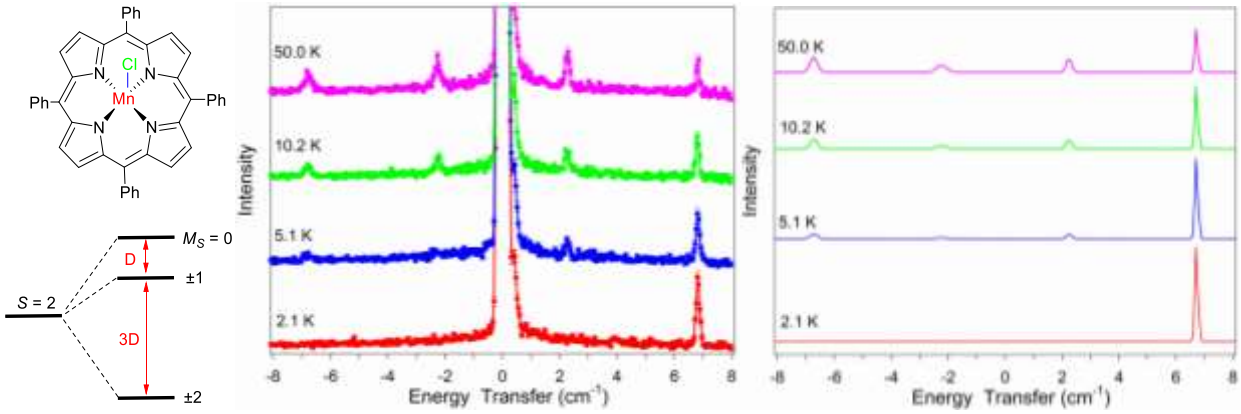

Figure 3. (Left) Mn(TPP)Cl and its ZFS splitting ($D < 0$). (Middle) INS spectra of [Mn(TPP)Cl] using a 12.58 cm^{-1} incident neutron beam[6g] at Cold Neutron Chopper Spectrometer (CNCS), SNS.[25] (Right) Theoretical INS spectra of an $S = 2$ spin system with D = -2.24(3) cm^{-1}.

Reprinted with permission by …

There are three types of INS instruments:[1d] direct-geometry TOF spectrometers, indirect-geometry TOF spectrometers, and triple-axis spectrometers (TAS). TOF spectrometers have been widely used for INS relevant to coordination chemistry, especially that of complexes, and powders are the most likely form of the samples. We will focus on these instrument types and briefly discuss TAS where applicable.

Designs of the direct- and indirect-geometry spectrometers are given in Scheme 3. In a direct-geometry spectrometer, the selected incident energy E_i is fixed and E_f is measured by TOF (Scheme 3-Left) to determine the energy transfer ($\hbar\omega = E_i - E_f$).[5b] Such a design allows for a wide range of $\boldsymbol{Q}$ measurement for different excitations. Direct-geometry instruments may also permit the use of a magnet and other ancillary equipment. Examples of such instruments at US facilities are the Cold Neutron Chopper Spectrometer (CNCS)[25] and the Fine-Resolution Fermi Chopper Spectrometer (SEQUOIA)[26] at SNS, ORNL and the Disk Chopper Spectrometer (DCS, NIST)[27] are examples of direct geometry instruments in the USA. Currently, the spectrometers at SNS (CNCS and SEQUOIA) and NIST (DCS) can be used with an 8-T and 11.5-T magnet, respectively.

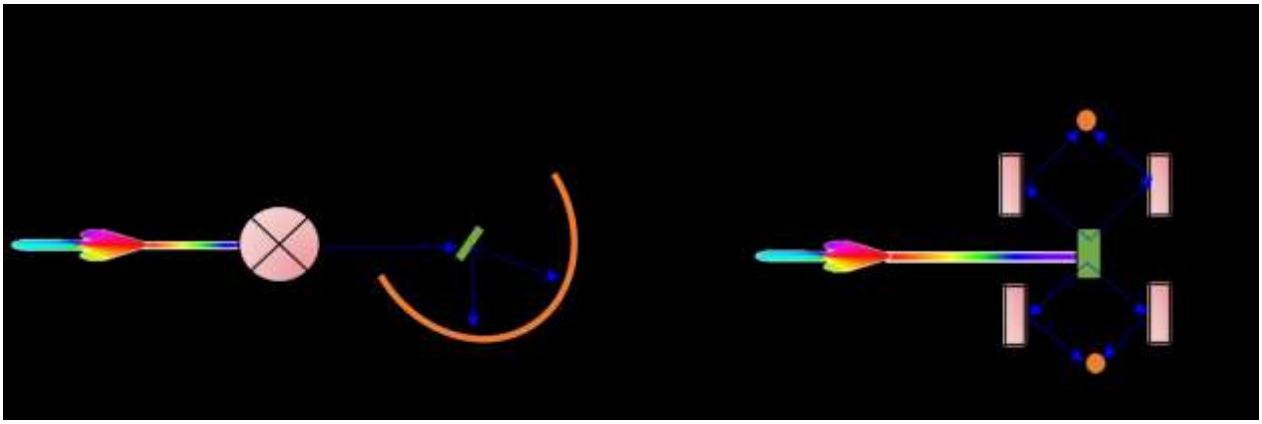

Scheme 3. (Left) Direct- and (Right) Indirect-geometry INS spectrometers. The indirect-geometry spectrometer is shown with scattering angles of 45° and 135°, forward scattering and backscattering, respectively (blue lines).

INS, in particular the scattering by the direct-geometry spectrometers that measure over a range of $\boldsymbol{Q}$, is unique in that it is capable of distinguishing magnetic peaks from those of vibrations.[1a, 5] Peaks of magnetic excitations in INS spectra *decrease* in intensity with increased $|\boldsymbol{Q}|$, while those from vibrations *increase* in intensity with increased $|\boldsymbol{Q}|$[1a, 5] An example is given for the INS spectra of Fe(TPP)Cl (S = 5/2, Figure 4).[6g] Changes in peak intensities vs $|\boldsymbol{Q}|$ are given in Figure 4-Right, showing that the intensity of the 12.65(8) cm^{-1} magnetic peak decreases with increased $|\boldsymbol{Q}|$. Intensities of the peaks that are >16 cm^{-1} increase with increased $|\boldsymbol{Q}|$,indicating that these peaks are vibrational in nature.[6g]

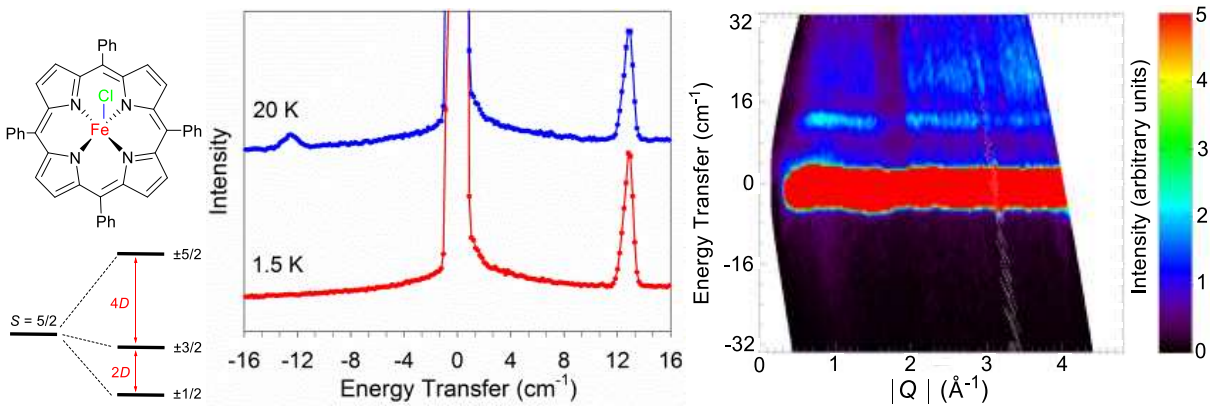

Figure 4. (Left) Fe(TPP)Cl and its ZFS splitting ($D > 0$). (Middle) INS spectra of Fe(TPP)Cl using a 24.20 cm^{-1} incident neutron beam[6g] at CNCS.[25] (Right) Change in the peak intensities vs $|\boldsymbol{Q}|$ at 1.5 K. Incident neutron energy: 80.66 cm^{-1}. Reprint with permission by the American Chemical Society.

For the indirect-geometry INS spectrometers, the final energy, E_f, of the scattered neutrons reaching the detectors are fixed by design (through crystal diffraction and/or filters). The incident neutrons can be either chosen individually, such as at a reactor source with a monochromator [such as FANS at NIST (US)[28] and IN1-LAGRANGE[29] at ILL (France)] or using a "white" beam where E_i is determined using the time the neutron reaches the detector through TOF.[1d] The latter, such as indirect-geometry INS spectrometers at spallation sources, gives a wide energy transfer range up to ca. 4000 cm^{-1} with high energy/spectral resolution.[30] The geometry of these instruments are such that E_i is much larger than E_f, thus making $\boldsymbol{Q}$ almost equal to $\boldsymbol{k_i}$ irrespective of the scattering angle and yielding limited $\boldsymbol{Q}$ information. The Vibrational Spectrometer (VISION,[30a] ORNL) is an example of an indirect-geometry instrument. There are two banks of analyzers (Scheme 3-Right) with two different scattering angles, one at 45° (forward scattering) and another at 135° (backscattering) giving two spectra per experimental data acquisition.

In a triple-axis spectrometer (TAS), monochromic neutrons interact with the sample and the E_f reaching the detector is selected by an analyzer.[1d] Because of the monochromic nature, incident neutron flux is not large. Since background noise from incoherent scattering of H atoms is large for H-containing materials, TAS is typically reserved for the study dispersion of excitation in the materials that do not contain H atoms. The MACS (Multi-Axis Crystal Spectrometer)[31] at NIST has characteristics of a triple-axis instrument.

1.2.3. Quasielastic Neutron Scattering (QENS)

QENS is a limiting case of INS, when energy transfers are very small compared to the incident neutron energy.[32] It is used to probe very small energy exchanges near the elastic line ($E = 0$), such as translational or rotational motion of atoms or molecules, that cause broadening of the elastic peak. Figure 5 is an example of QENS spectra of a Cu-Tb based single-molecule magnet (SMM).[33] At 3.5 K, the spectrum is almost completely elastic. With temperature increase, the bottom of the spectra becomes broader, which is attributed to a distinct magnetic relaxation on the ns-ps timescale. This is *faster* than the magnetic relaxation observed by AC susceptibility on the ms timescale around T = 2 K.[33] High-resolution spectrometers, such as Backscattering Spectrometer (BASIS) at ORNL and High Flux Backscattering Spectrometer (HFBS) at NIST,[34] are typically required for QENS, but any direct-geometry TOF instrument such as CNCS[25] and DCS[27] can also be used. Recently QENS spectra of $Co(acac)_2(D_2O)_2$, another SMM, at BASIS with a 4-T magnet reveals that the rotation of the methyl groups on the acac ligands is slowed down by the magnetic field increase.[35]

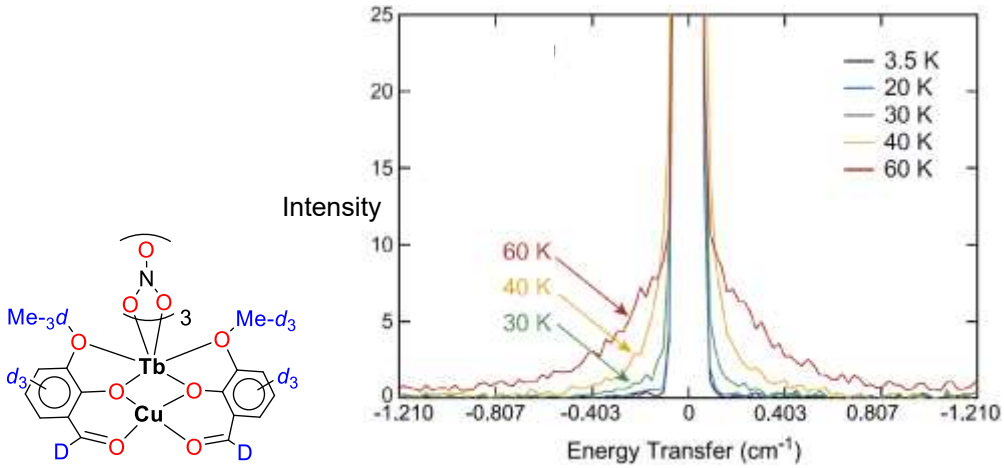

Figure 5. (Left) Structure of a Cu-Tb complex; (Right) QENS spectra at variable temperatures.[33] Reprinted with permission by Elsevier.

2. Single-Crystal Diffractometers

Single-crystal neutron diffraction gives precise determination of the structures of the samples. There are two single-crystal neutron diffractometers at ORNL suitable for chemistry. TOPAZ (BL-12)[36] at the SNS uses neutron wavelength-resolved TOF Laue technique for data collection,[2] while HB-3A Four-Circle Diffractometer (FCD)[37] at HFIR uses constant monochromatic neutrons at HFIR.[3]

TOPAZ is a high-resolution single-crystal diffractomer for chemical crystallography. In comparison to FCD, TOPAZ offers better real space resolution and is more suitable for molecular structures with unit cell lengths up to 70 Å.[21] Hydrogen atom positions can be well resolved from data collected on TOPAZ. *No* deuteration of samples is often needed for diffraction on TOPAZ, making it much easier to obtain crystal structures of coordination compounds. TOPAZ is not equipped with a magnet. FCD is efficient for more focused research to answer, e.g., a specific question after the structure of the molecule has been determined by X-ray diffraction. It provides nuclear and magnetic structures as a function of temperature T (~0.05-

800 K), pressure P (0-100 kbar), magnetic field B (0-8 T), and electric field E (0-10^4 V/cm).

2.1. TOPAZ at ORNL

Neutron wavelength-resolved TOF Laue technique is employed at TOPAZ,[36] expanding the measured diffraction pattern from 2D on detector faces to wavelength-resolved 3D volume in (x, y, λ) along the neutron TOF direction. The instrument is capable of volumetric reciprocal space mapping to high resolution, Q_{max} = 25 Å^{-1} (d_{min} = 0.25 Å), the highest in resolution among the suite of neutron single-crystal diffraction instruments at HFIR and SNS. Single-crystal samples with dimensions between 0.1-3 mm on edge and a volume of 0.1–30 mm^3, preferably isometric, are well suited for TOPAZ. The newly installed high-flux neutron guide enables routine measurements of submillimeter size single-crystal samples. A data set can be collected at ambient conditions or in controlled sample environments within couple hours or up to 6 days, depending on the sample size, composition, unit cell volume, crystal symmetry, and diffraction quality. A cold flow from liquid nitrogen with a temperature range of 90–450 K provides sample cooling and heating. Delivery of a low-temperature (5 K) goniometer is anticipated by 2019. It is worth noting that a large continuous 3D volumes of neutron diffraction data can be measured on a single sample position and saved in event mode. Such a design is ideal for variable-temperature study of structural/magnetic phase transitions in real time. Event data can also be collected under applied electric field under static or stroboscopic conditions for parametric studies. Future upgrade plans for TOPAZ also include a diamond anvil cell for pressure study of small single-crystal samples (<0.05 mm^3 in volume).

In the short time since TOPAZ became operational, it has been widely used in coordination chemistry studies. The broad Q coverage (Q_{max} = 25 Å^{-1}) makes TOPAZ ideal for

studying nuclear and magnetic structures at subatomic resolution. Examples span a wide range of inorganic materials, including position assignment of Fe and Co centers in a heterometallic mixed-valent molecular precursor,[38] hydrogen bonding in hybrid inorganic-organic perovskites,[39] and guest-host interaction in uranyl nanoclusters.[40] Neutron diffraction at TOPAZ has confirmed the long sought-after β-agostic bond between a C–H bond and late transition metal ion Pd(II) that has eluded structural characterization for decades.[41] Position of the agostic hydrogen could not be located directly from the differential electron density map using X-ray diffraction because of the low electron density of the hydrogen atom in contrast to the heavy Pd(II) ion. A hydrogenated single-crystal sample of suitable sizes works well on TOPAZ. A few other cases of TOPAZ use in coordination chemistry work are given below.

Synthetic biologically inspired complexes exhibiting reactivity similar to hydrogenase enzymes have provided evidence of hydride transfer to the metal and proton transfer to an amine, but key structural information about the intermediate is not readily discernible with X-ray diffraction.[42] Bullock et al. reported the cleavage of dihydrogen bond using a synthetic mimic of [FeFe]-hydrogenase [*Cp*FeN-*L)*](BARF) (*Cp* = pentafluoropyridylcyclopentadienide; N-*L*= 1, 5-di(*tert*-butyl)-3,7-di(*tert*-butyl)-1,5-diaza-3,7-diphosphacyclooctane; BARF = B[3,5-$(CF_3)_2C_6H_3]_4^-$), under mild conditions.[43] Experimental data from the iron complex suggests that the pedant amines act as proton relay to accelerate intra- and intermolecular proton transfer and facilitating coupled proton-electron transfer reaction for electrocatalytic oxidation of H_2.

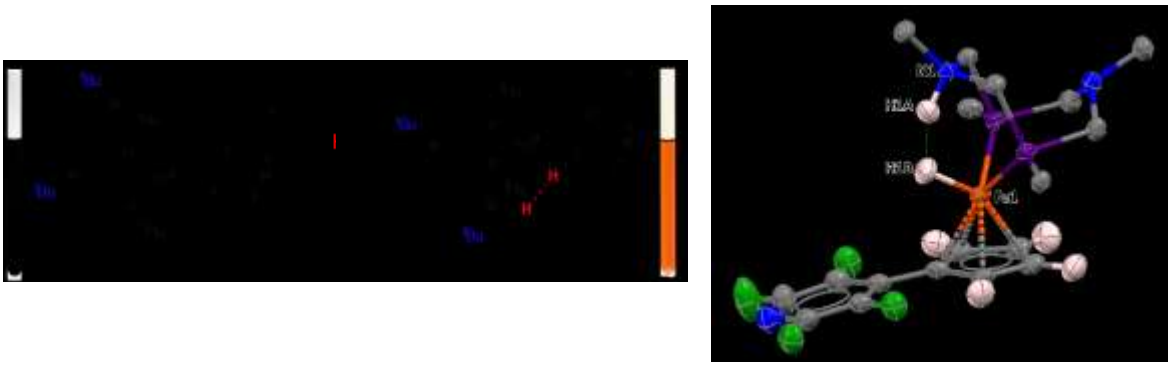

Figure 6. Molecular structure of [C*p*FeH···HN-*L*]$^+$ determined by neutron diffraction, showing thermal ellipsoids at 50% probability level.[44] For clarity, the methyl substituents of the P^{t}Bu$_2$(N^{t}Bu$_2$) ligand, the BArF$_4^-$ anion, the co-crystallized fluorobenzene molecule, and hydrogen atoms bonded to carbon atoms are omitted. Selected H-bond distances (Å): H1A···H1B 1.489(10); Fe1–H1B 1.544(7); N1–H1A 1.079(6); H1B–H1A–N1 155.6(8).

The neutron structure measured on TOPAZ confirms that reaction of [*Cp*FeHN-*L)*]$^+$ with H_2 under mild conditions leads to heterolytic cleavage of the H-H bond into a proton and hydride (Figure 6).[44] The precise location of H atoms in the reaction intermediate [C*p*FeH···HN-*L*]$^+$ reveals remarkably short H···H distance of 1.489(10) Å, documenting an unusually strong "dihydrogen bonding" interaction between the acidic N–H$^{\delta+}$ and hydridic Fe–H$^{\delta-}$, where the ferrous hydridic site {Fe(II)-H$^-$} acts as the H-bond acceptor and the nitrogen of the protic pendant amine {*L*-N-H$^+$} as the H-bond donor. The neutron structure provides clear evidence of a crucial intermediate involving an Fe-H···H-N interaction in the oxidation of H_2. The result clarifies the key role of the pendant amine in the iron complex and provides insights into the design of synthetic electrocatalysts sought as cost-effective alternatives to platinum in fuel cells.

Another example is the study of polyhydrido copper nanoclusters by TOPAZ. Metal hydride clusters are an important class of materials for hydrogen related applications. Central to

this work is the hydride ligand, H^-, the smallest closed-shell anion known. Dhayal *et al.* reported a $[Cu_{32}(H)_{20}\{S_2P(O^iPr)_2\}_{12}]$ nanocluster containing the highest number of hydrides in a molecular cluster.[45] The positions of 20 hydrides of the $Cu_{32}H_{20}$ core were well resolved from high resolution data collected on TOPAZ for a 0.45 mm^3 single-crystal sample with more than 51 atom% hydrogen (Figure 7). The polyhydrido copper cluster studied consists of 12 tri-, 6 tetra-, and 2 penta-coordinated hydrides in capping and interstitial modes.[46] It is noted that diffraction from a much *smaller* single crystal of 0.065 mm^3 on TOPAZ successfully located the hydride positions in another hydrogenated nanospheric polyhydrido copper cluster.[47]

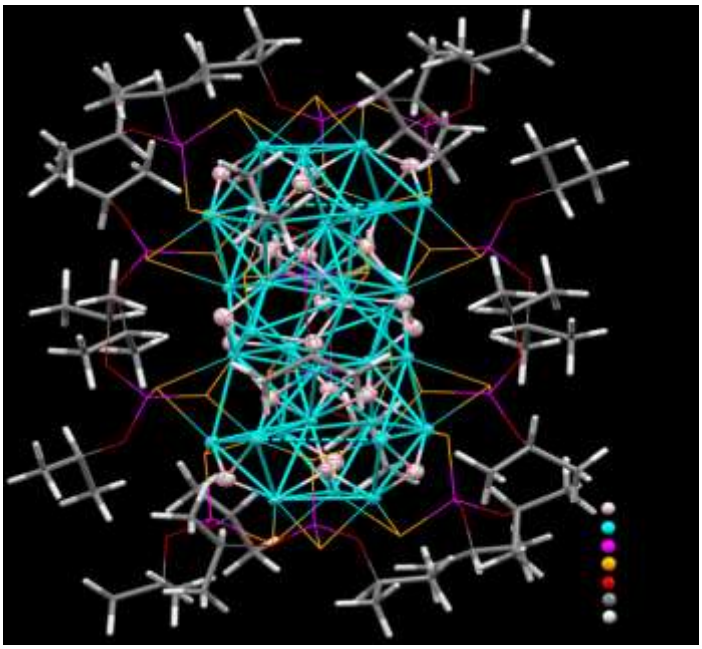

Figure 7. The positions of 20 hydrides of the $Cu_{32}H_{20}$ core were well resolved from high resolution data collected on TOPAZ for a 0.45 mm^3 single-crystal sample with more than 51 atomic% hydrogen.[46]

2.2. Four Circle Diffractometer (FCD, also known as HB-3A) at ORNL

Four-Circle Diffractometer (FCD, HB3A) at HFIR is a single-crystal neutron

diffractometer equipped with a 2-D Anger Camera detector.[37] A bent perfect silicon monochromator can vary the incident neutrons from high flux (2.2×10^7 ns/cm^2/s) to high resolution mode ($\delta \boldsymbol{q}$ = 0.007 Å^{-1}, corresponding to ~900 Å size scale; $|\boldsymbol{q}| = 2\pi/d$; d is a real space distance) for various scientific missions, ranging from weak scattering signals (small required crystal size of sub-mm or weak magnetic/superlattice order) to weak lattice distortions or large-scale magnetism such as long periodicity helical and skyrmion lattice. The monochromator can select three wavelengths of 1.008 Å, 1.5503 Å, and 2.551 Å, and can reach the highest atomic resolution of 0.504 Å. As indicated earlier, the main mission of FCD is to explore nuclear and magnetic structures as a function of temperature, pressure, magnetic field, and electric field. FCD aims to understand phases emerging from competing interactions among spin, charge, orbital, and lattice degrees of freedom. Studies cover physics, chemistry, materials science, and mineralogy.

The high flux/resolution monochromatic thermal neutron beam at FCD is a distinctive feature, which is good for precisely and efficiently measuring small unit cell crystallographic and magnetic structures (<10^4 Å). The large, 2-D Anger camera detector provides the capability for efficiently surveying the full q-space under complex sample environment and also half-polarized neutron diffraction to detect magnetic anisotropy. Benefiting from the different scattering lengths than X-rays, it is more efficient to use FCD jointly with single-crystal X-ray diffraction for crystallographic and magnetic structure studies, such as new materials in solid state chemistry, complex molecular magnetism, and phase analysis of complex phase transitions and phase coexistence, especially those requiring complex/combined sample environment. The typical size of crystal has a side length of 0.5-5 mm. The instrument is efficient to solve the phase transition versus temperature, fields, pressures, especially for small unit cell structures.

Examples of the FCD use includes the structure determination for uranium aluminide silicide $U_8Al_{19}Si_6$, a stuffed supercell grown from aluminum flux by Latturner's group.[48] Al and Si, next to each other in the periodic table, is difficult to be distinguished by X-ray diffraction. Both UAl_3 and USi_3 adopt the cubic $AuCu_3$ structure type. However, $U_8Al_{19}Si_6$ has a stuffed superstructure reportedly isomorphous to cubic UAl_3 and USi_3. However, neutron diffraction at FCD revealed that $U_8Al_{19}Si_6$ ($Z = 8$, $Pm\text{-}3n$) is a new stuffed supercell variant of UAl_3. It has 4 times the expanded unit cell along each cubic axis than that for UAl_3 or USi_3 and also two extra occupied sites for Al/Si, the so-called stuffed sites (Figure 8), resulting in a U:(Al/Si) ratio of 1:3.125 instead of the expected 1:3. The neutron diffraction was used to distinguish ordered Al and Si sites. The neutron data were interpreted with the X-ray data collected from the part of the same piece of crystal at 150 K, giving the structure in Figure 8.[48] Combined single-crystal neutron and X-ray diffraction studies have also led to the determination of $Yb_{3-\delta}FeAl_{4-x}Mg_xSi_2$ to confirm atom positions and occupancies, including the extent of substitution.[49]

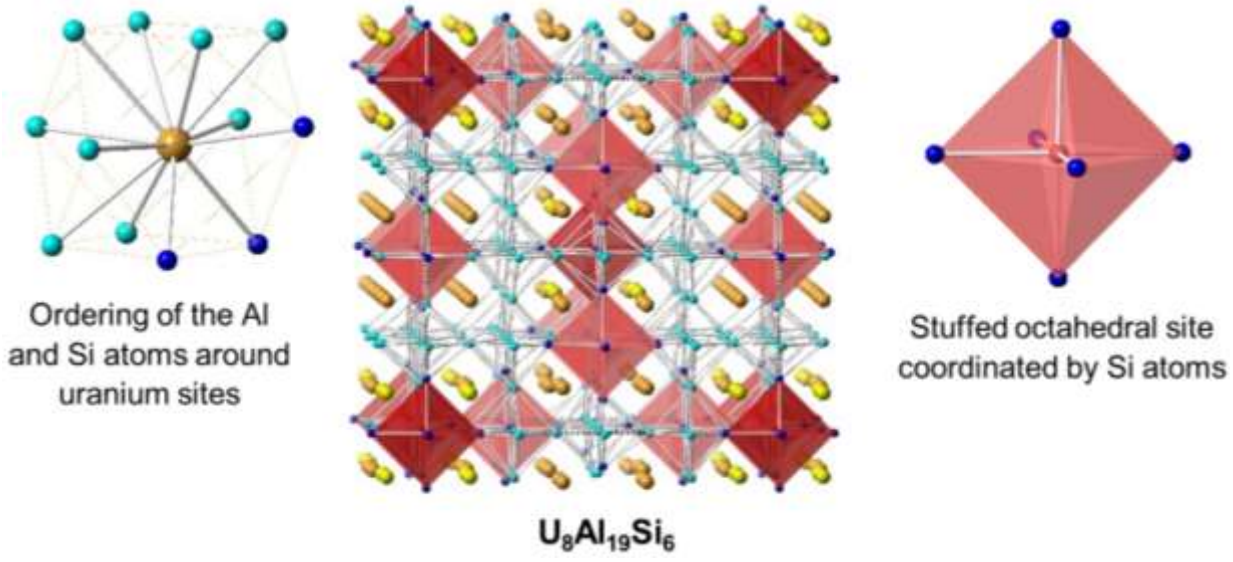

Figure 8. Crystal structure of $U_8Al_{19}Si_6$ determined by single-crystal neutron diffraction at

FCD.[48] U (yellow and red inside the stuffed sites), Al (light blue), Si (dark blue). Reprinted with permission by the American Chemical Society.

FCD is mostly used for calibrating magnetic orders in solids, such as the $[MnSb_4]^{9-}$ cluster in $Yb_{14}MnSb_{11}$,[50] and the magnetic structure of $EuCo_2As_2$, indicating ordered magnetic moments only on Eu sites.[51] FCD has also been used in the atomic displacement studies that are related to structural transition, instability, anharmonicity, and thermal or quantum fluctuations.[52]

Single-crystal diffractometers around the world that are similar to TOPAZ using TOF Laue include SXD[53] at ISIS (UK), SENJU[54] at J-PARC (Japan), and thermal neutron Laue diffractometers FALCON[55] at HBZ (Germany), Koala[56] at ANSTO (Australia) and VIVALDI[57] at ILL (France). In addition to TOPAZ, the suite of single-crystal instruments at SNS (ORNL) include the Elastic Diffuse Scattering Spectrometer (CORELLI),[58] Macromolecular Neutron Diffractometer (ManDi),[59], and Spallation Neutrons and Pressure Diffractometer (SNAP).[60]

Diffractometers similar to FCD include D9[61] and D10,[62] both at ILL (France), HEiDi[63] at FRM-II (Germany), ZEBRA[64] at PSI (Switzerland), and BL18[65] at J-PARC (Japan).

3. Powder Diffractometers

In the absence of suitable single crystals, solving or refining crystal structures requires the use of powder diffraction. At any particular neutron facility, often several styles of powder diffractometer cater to a specific requirement for types of problems that can be solved. The most practical for structure solution are high-resolution instruments. Three powder diffractometers,

General-Purpose Powder Diffractometer (POWGEN)[66] at SNS, ORNL, High-Resolution Powder Diffractometer (BT-1)[67] at NIST, and Neutron Powder Diffractometer (POWDER, HB-2A)[68] at HFIR, ORNL are discussed below. Pulsed neutrons from spallation are employed at POWGEN, while BT-1 and HB-2A use neutrons from steady-state reactors.

These instruments are generally characterized by narrow instrumental resolution over a large Q-range ($Q = 4\pi \sin\theta / \lambda$, where λ is the wavelength and θ is the scattering angle) that allows for the best chance of resolving Bragg peaks, even for low crystal symmetry materials, and resulting in high accuracy of extracted structural parameters. These types of instruments are usually flux-limited, leading to data collection times on the order of hours. If speed of data collection is a priority, instruments have been designed that reduce the Q-range, and/or coarsen the instrument resolution, increasing the flux on sample by several orders of magnitude in comparison to a high-resolution instrument. When coupled with a large 2-dimensional detector, it is possible to record diffraction patterns in the sub-second regime, allowing for kinetic processes to be measured.

Preparing samples for neutron powder diffraction is typically straight forward after ensuring phase-purity and crystallinity using a laboratory X-ray powder diffractometer. The sample is then loaded in to a suitable vanadium-alloy or null-scattering cell which exhibits either small, or no Bragg peaks for neutrons. The cell is not completely transparent to neutrons as there is a substantial incoherent scattering from vanadium, adding to the background. Weak scattering of small samples may benefit from using aluminum as a cell that reduces the background, but will generate Bragg peaks in known locations, and can benefit magnetic structure determinations. Regular helium-flow cryostats, or closed-cycle displexes, and furnaces can be used to control temperature with some consideration given to either ensuring the sample is not sealed gas-tight

and that the cryostat sample space has sufficient helium for thermal exchange, or that the sample cell is sealed under a helium environment. Another cell option for samples needed to obtain mK temperatures is a copper can capable of being pressurized with helium to about 10 bar at room temperature, where the copper is necessary to ensure thermal conductivity. Use of magnets further requires that non-magnetic screws and adaptors be used.

Analyzing the powder diffraction data can be practically separated into two parts. The Bragg peak locations are determined by instruments factors (zero-point error, wavelength) and the material space group and unit cell dimensions. The intensities of the Bragg peaks concern the exact distribution and location of isotopes in the unit cell with attenuation due to atomic displacements parameters (ADP's or Debye-Waller factors) and perhaps more detailed considerations such as preferred orientation and stacking faults. If only the unit cell size is required from the data, a whole-pattern fitting process (Pawley[69] or Le Bail[70] amongst other intensity extraction techniques) is performed. If the structure is known or close to being known, a Rietveld analysis[71] can be undertaken, where a structural model is built and manipulated to best match the data. Alternatively, partial or full structure solutions[72] must be performed using the myriad of techniques and software available (e.g., GSAS-II,[73] FULLPROF,[74] and TOPAS[75]) from the peak intensities extracted in profile fitting or from simulated-annealing and Monte-Carlo-type or Charge Flipping approaches.

3.1. POWGEN at ORNL

POWGEN[66] is a third-generation, TOF powder diffractometer at SNS.[76] This instrument was designed with high flexibility of operation, whereby the user can use a range of incident wavelengths by adjusting the bandwidth limiting choppers and pulse repetition rate. The

incident wavelength chosen dictates the range of *d*-spacing or *Q* covered within the spectrum. It is possible to access a *d*-range of 0.1-ca. 30 Å using multiple measurements, making this suitable for the study of a wide variety of inorganic materials such as oxides, hydrides, MOFs, and zeolites. The access to long *d*-spacing also makes the instrument suitable to study magnetic structures of a variety of materials. Within a single measurement, it is also possible to obtain data from d = 0.5-14 Å, making POWGEN an ideal instrument to carry out in-situ/in-operando neutron powder diffraction. Examples include cycling of batteries, chemical looping reaction, oxidation-reduction reaction, sample synthesis and much more.

The location of the detectors in the instrument allows for all detected scattered neutrons to be focused onto a single diffraction profile yielding high count rate with variable resolution ranging from $\Delta d/d$ = 0.0006 to 0.02. Some of this resolution can be traded for higher intensity using a movable guide section. The high intensity guide gives a factor of 1.2, 1.8 and 2.2 gain at center wavelength 0.8, 1.5 and 2.665 Å, respectively at 60 Hz making it possible to collect data from smaller samples. Typical samples sizes range from 1 to 3 cm^3. Data collection time varies from minutes to hours depending on amount, crystallinity, symmetry of structure and elemental composition of sample.

POWGEN has an extremely versatile portfolio of science, most of which involves inorganic compounds.[66] One community with a large user base is researchers working on Li-ion batteries. Li is a light element and as such accurate structural information about Li^+ is hard to characterize with more traditional techniques including X-ray diffraction especially in the presence of other heavier elements such as transition metals (TM) and lanthanides for example. In addition, many candidates tend to be oxides and have a mixture of TM in the same crystallographic site, which again is difficult to distinguish by X-ray diffraction alone due to

their similar scattering power. In a series of studies,[77] spinel-based cathodes with nominal formula $LiNi_{0.5}Mn_{1.5}O_4$ were structurally characterized using average and total scattering methods. Li-ion batteries with higher voltage cathodes could increase the energy density by 20-50%. Their practical use is thwarted by narrow electrochemical window of existing liquid electrolyte, poor safety, capacity fade, limited cycle life, solid electrolyte interphase (SEI) formation and dissolution of transition metals from cathodes. One possible solution is the use of a solid electrolyte. One candidate is the garnet-based $Li_{6\pm d}La_3Zr_2O_{12}$. Neutron and X-ray diffraction helped define the carrier concentration for a family of compounds with Ta doping in the Zr site.[78]

Materials which store and release oxygen as they convert between different phases and crystal structures are often called oxygen-storage materials (OSM).[79] They can be used in chemical looping reactions such as methane reformation to capture CO_2 and simultaneously produce H_2 (Figure 9). Such a process has the potential to efficiently capture CO_2 in the case of chemical-looping combustion or generate syngas ($CO + 2H_2$) in the case of chemical-looping reforming (CLR).[79] A major factor that determines the performance of these materials is the transport of oxygen between the bulk and the surface of the OSM. The chemical looping reaction generally takes a few minutes to cycle. Thus, a fast diffraction technique such as synchrotron X-ray diffraction (SXRD) had been used to follow various structural phase transitions. A team from the University of Maryland carried out neutron powder diffraction on samples of $La_{1-x}Sr_xFeO_{3-d}$, a potential candidate for OSM, using the gas-handling system at POWGEN, which enabled alternating flows of 15% CH_4 in N_2 and air (20% O_2 in N_2) over the sample while measuring neutron diffraction patterns at a variety of temperatures of 135-835 °C for four different sample compositions (x = 0, 0.5, 0.67 and 1, Figure 9).[79b] While kinetics and structure can be easily

followed using SXRD, it is still difficult to determine accurate oxygen stoichiometry due to the presence of much heavier Sr and Fe in the sample. Using X-ray and neutron powder diffraction to analyze the structure under operational condition, the team conclude that each material in this series has an "envelope" of oxygen storage capacity over a certain temperature range. Oxygen can easily and reversibly be inserted and removed from the material in this range. However, kinetic limitations keep the lattice oxygen inaccessible to cycling and above this region, the difference in oxygen content for the material under oxidizing and reducing conditions is negligible.

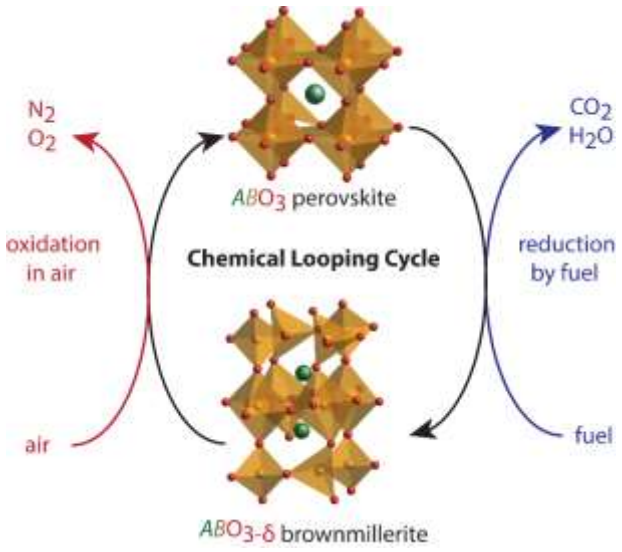

Figure 9. Schematic representation of the chemical-looping process (top). Here, a perovskite is alternatingly exposed to air and a fuel (e.g., methane) to cycle the material.[79b] Reprinted with permission by the American Chemical Society.

A new clathrate type was discovered in the Ba/Cu/Zn/P system by the Kovnir group at the University of California at Davis. The crystal structure of the $Ba_8M_{24}P_{28+\delta}$ (M = Cu/Zn)

clathrate is composed of the pentagonal dodecahedra common to clathrates along with a unique 22-vertex polyhedron with two hexagonal faces capped by additional partially occupied phosphorus sites. This is the first example of a clathrate compound where the framework atoms are not in tetrahedral or trigonal-pyramidal coordination. Due to the similarity of X-ray scattering lengths for Cu and Zn, neutron diffraction data collected at POWGEN was crucial to solve the crystal structure of this material. Low thermal conductivity, a tunable composition, and tunable charge transport properties make the title compound a promising base for the development of novel thermoelectric materials (Figure 10).[80]

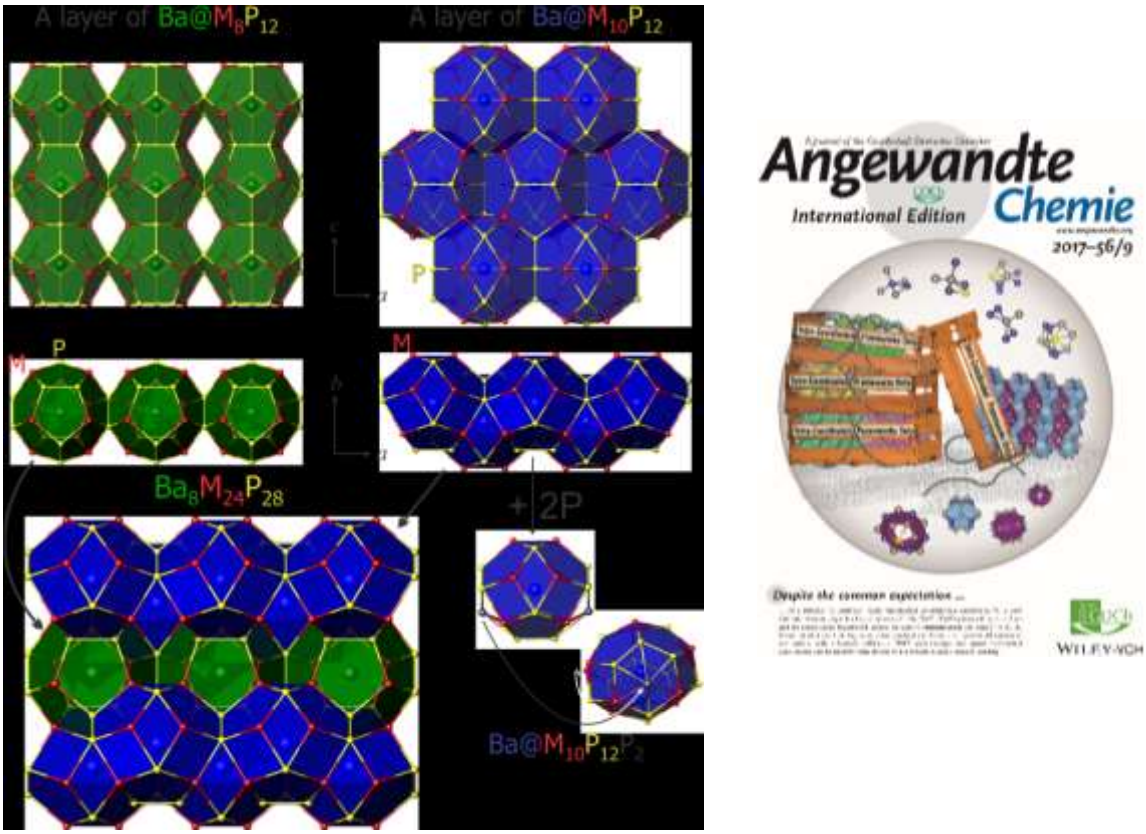

Figure 10. Polyhedral representation of the crystal structure of $Ba_8M_{24}P_{28+\delta}$. Ba: green and blue; M: red; P; yellow and grey.[80]

3.2. BT-1 at NIST

BT-1, built in 1992,[67, 81] is a high-resolution powder diffractometer. In the current configuration, the incident wavelength, resolution, and *Q* range is defined by the primary beam collimation choice, focusing monochromator choice, pre-sample collimation, and the detector collimation. The most frequently used set-up for a coordination polymers and metal-organic framework is to use the most open primary beam and the Ge(311) monochromator (λ = 2.078 Å, $Q_{max} \approx 6$ Å^{-1}) to give the highest flux, and good resolution between 0.011 Å^{-1} and 0.015 Å^{-1} up to a *Q* of ca. 4.5 Å^{-1}. The lowest flux, highest resolution Ge(733) monochromator is infrequently used, while the Cu(311) monochromator is excellent for smaller unit cells (lattice parameters under ca. 10 Å). Typical sample cell volumes are 1-10 cm^3, with negligible resolution dependence on sample size. Counting times for Rietveld quality data depend on the sample size. For example, a few hundred milligrams of a well crystalline MOF, a full pattern can be acquired in 6 to 8 h. In addition, most samples retain their intrinsic H-containing ligands, and relatively few samples are deuterated for measurement on BT-1. Rietveld quality data have been taken on materials that are on the order of 50 atom% hydrogen on BT-1, making the diffractometer comparable with other monochromatic instruments.[82]

The range of sample environments that control temperature on BT-1 are given in Table 1. Several of these can be used with other ancillary equipment such as gas dosing (to 300 bar), application of electric field for closed-cycle refrigerators (CCRs), or application of isotropic gas pressure to 12 kbar with top-loading CCRs or helium-flow cryostats. Of interest to magnetic systems is the 7-T vertical-field magnet that can operate with a top-loading CCR and a He-3 dipper to reach 300 mK. Given compatibilities of stray fields and temperature controlling equipment, the use of a 10-T or 11.5-T magnet is needed for the dilution refrigerator inserts to

allow sample temperatures to reach 50 mK, but the maximum fields are limited to 4 T.

Table 1. Temperature capabilities of the various sample environments compatible with BT-1. Bottom-loading CCRs operate with the sample space under vacuum. Top-loading CCRs can run below room temperature with He exchange gas, but must operate under vacuum at higher temperatures. Top-loading CCRs typically have different thermometry on the sample sticks for low or high temperature uses.

Environment	**Temperature Range (K)**	**Sample cell requirements**
Dilution refrigerator insert	0.05-300	Cu, under 10 bar He-4
He-3 (dipper or dedicated)	0.3-300	V, Al, or Cu
Liquid He-4 cryostat	1.5-300	V preferred
Bottom-loading CCR (high power)	3-325	V preferred
Bottom-loading CCR (low power)	6-325	V preferred
Bottom-loading high temperature CCR	14-800	V preferred, Cu lid preferred, appropriate seals for temperature range needed
Top-loading CCR	5-700	V preferred, Cu lid preferred, appropriate seals for temperature range needed
Furnaces	300-1873	Discussion with a local scientist is needed

Powder diffraction is one of the workhorse techniques, as it is fundamental to understand the arrangements of atoms in materials and how functions of the materials is derived from the structure. The BT-1 powder diffractometer contributes data for about 30-40 publications each year. The data from this instrument has played an important role in understanding the structures of MOFs with interesting structural and mechanical features,[83] and their gas adsorption and separations properties. From single-component adsorption of industrially important small molecules such as water,[84] CO_2,[85] methane,[86] acetylene,[87] noble gases,[88] Cl_2 and Br_2,[89] and O_2[90] to combinations of these and other gases for separations processes.[91] From 2005[92] to mid-2018, there have been significant progress and understanding of how H_2 binds to MOFs,[93] and how the strong attraction of H_2 to an open metal site[94] can lead to increases in both the H_2 loading at temperatures above 77 K,[95] and the density of the adsorbed H_2.[96] Of importance to the practical operations of H_2 in a storage tank for vehicular use is to increase the storage capacity at temperatures approaching room temperature. One potential method is by overcoming the limitation of having only one H_2 molecule bind to each metal in these MOFs. Recently, a proof-of-principle example demonstrated that this concept is indeed possible.[97] Combining a thiolated $dsbdc^{4-}$ ligand ($dsbdc^{4-}$ = 2,5-disulfido-1,4-benzenedicarboxylate) and Mn^{2+} ions produces a porosity that is similar to the MOF-74 series which is based on the $dobdc^{4-}$ ligand ($dobdc^{4-}$ = 2,5-dioxy-1,4-benzenedicarboxylate) (Figure 11), but with important structural differences. In Mn_2(dsbdc), two different octahedral metal centers alternate down the helical chains parallel to the pore direction. One Mn^{2+} ion is ligated to 6 atoms from the framework and the other is ligated by 4 atoms with 2 solvents. Removal of the solvents yields a MOF with two potential adsorption sites on the same metal ion.

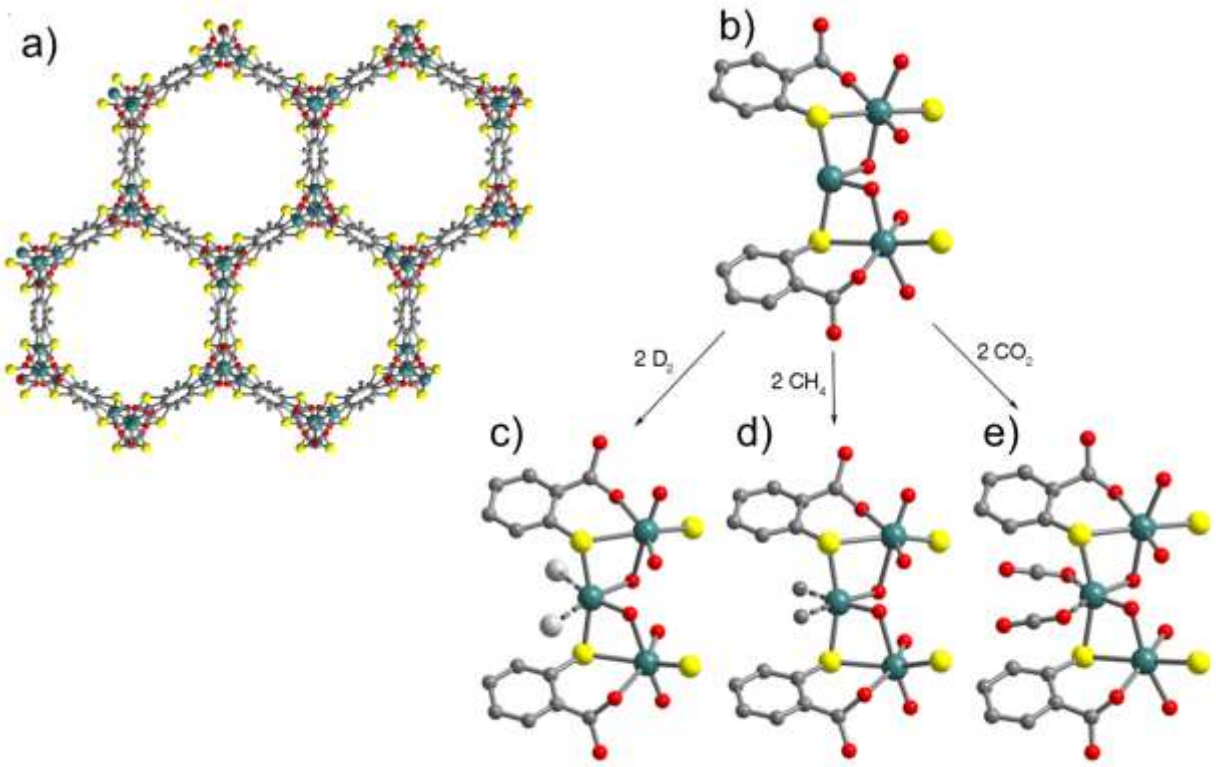

Figure 11. (a) The 1-D pore structure of activated Mn_2(dsbdc); S (yellow), C (green), O (red). (b) Local coordination around the two distinct Mn^{2+} ions (green) showing the closed octahedral coordination of one Mn^{2+} ion and the four-coordinate Mn^{2+} ion. (c) Binding of two D_2 molecules obtained from neutron powder diffraction. (d) and (e) show that CH_4 and CO_2 can also bind in the same coordination mode and identified through synchrotron X-ray powder diffraction.[97] Reprinted from Ref. [97] with permission by The Royal Society of Chemistry.

Coordination polymers have also been of interest due to their magnetic characteristics. Since neutrons are sensitive to the arrangement of magnetic moments and their dynamics in a material, the average magnetic structure can be determined by powder diffraction.[98] Using BT-1, several magnetic structures have been determined for coordination polymers exhibiting long-range antiferromagnetism.[99] Since these magnetic moments are usually small, the effort to

deuterate, or partially deuterate, these samples and to couple them with inelastic neutron scattering (INS) experiments to discern about the spin interactions, often pays dividends in improving signal to noise. Further, BT-1 is not optimized for weak magnetic scattering (under ca. 0.5 μB) or for scanning individual Bragg peaks as a function of temperature or field to obtain the order parameter for the magnetic phase transition. As such a high-flux triple-axis instrument equipped with a position sensitive detector (PSD) such as BT-7 at NIST,[100] is more efficient even if it is perhaps more appropriately, or commonly used, for measuring single crystals such as multiferroics.[101] The resulting diffraction patterns are coarser than BT-1, but the approximately 20 times increase in count rate is much more efficient. Some clear examples where BT-1 and BT-7 were used to obtain the full picture of structures and order parameters are from work on the iron-arsenic superconductors,[102] and magnetostrictive Laves phases.[103]

3.3. POWDER (also known as HB-2A) at ORNL

The HB-2A neutron powder diffractometer at HFIR[68] is primarily utilized for magnetic structure determination, with an emphasis on ultra-low temperatures combined with high magnetic field or pressure. As such, the instrument design offers a balance of good Q-resolution while still maintaining much of the high intensity flux from the HB-2 beam port.[68b] The constant wavelength is selected with a germanium monochromator. Two principle wavelengths are utilized. The longer 2.41 Å (Ge 113) wavelength offers access to lower Q (Q_{range} = 0.2-5.1 Å^{-1}) and improved background and resolution for magnetic structure studies compared those using the shorter wavelength. The shorter 1.54 Å (Ge 115) wavelength gives a wider Q coverage (Q_{range} = 0.35-8 Å^{-1}), to allow more detailed crystal structure refinements. The layout of HB-2A follows a Debye-Scherrer geometry with a detector bank with a full detector coverage of ca 150°.

Typical sample masses of 5 grams (or 1 cm^3) and above make optimum use of the large beam size of 60 × 20 mm^2 at sample. However, measurements on smaller samples are routinely performed with longer counting times. The counting times to achieve Rietveld quality data vary between samples, but can generally be achieved under an hour. H-containing samples will require longer counting times, while deuteration reducing the large H-background is often required to observe magnetic reflections. Timescales for magnetic measurements range from under an hour up to 12 hours on small samples with weak or diffuse magnetic signals. To further complement magnetic studies, HB-2A has implemented a polarized incident neutron beam option offering extreme sensitivity to small magnetic signals (<0.1 μ_B) in powder materials with ferromagnetic or ferrimagnetic components to the moment.[104]

HB-2A has an impressive variety of sample environments to access the required temperature, magnetic field, and pressure phase diagrams. The open instrument layout, combined with the well understood and flat background from the monochromatic beam, allows for the easy switching between the different sample environments. Sample environments include ultra-low temperature measurements in dilution (50 mK) and ^{3}He (280 mK) inserts, applied magnetic fields (6 T), and pressure cells (19 kbar, with an available cylindrical sample space of 10 mm diameter and 25 mm height) that are routinely performed along with traditional cryostats (1.5 K) and air or vacuum furnaces (up to 1800 K). Room temperature measurements on multiple samples can be performed with a 6-carousel sample changer. A 3-sample stick has recently been implemented into the orange cryostat (1.5-300 K), with similar capabilities for other sample environments under development.

HB-2A is a workhorse powder diffractometer covering diverse science areas with the core focused on the investigation of magnetic structures. The detailed analysis of complex

magnetic structures often requires advanced techniques, such as representational analysis or magnetic symmetry techniques. General examples include quantum critical phenomena,[105] magnetism in multiferroic materials,[106] low-dimensional magnetism,[107] strongly correlated materials with large spin-orbit interactions and coupling between magnetism and lattice or electronic conduction,[108] and thermoelectric materials.[109]

In terms of coordination chemistry, HB-2A has been utilized primarily to access the magnetic structures of the compounds.[110] Hydrogen atom is a strong incoherent scatter for neutrons and therefore adds a large background to measurements of hydrogen-continuing compounds, which has to be considered when dealing with often small signals from magnetic scattering. To mitigate this, deuteration is often necessary to remove the background. Nevertheless, several measurements of materials with high hydrogen content have been successfully performed on HB-2A, with the example below (Figure 12), one such case of a compound with high hydrogen content.

Neutron diffraction is the principle tool for determining magnetic structures since it gives access to the direction and size of magnetic moments and their periodic ordering in the lattice. This is typically done using an unpolarized neutron beam in the same manner as crystal structure determination, with measurements taken in the unordered paramagnetic regime and then at lower temperature (or altered field, pressure) in the ordered regime to observe the magnetic Bragg peaks indicative of long range order. However, a notable counter example using polarized neutron diffraction can be found in the study of the Prussian blue analog coordination polymer.[110c] Polarizing the incident beam and then controlling the direction of an applied field allows highly sensitive access to ferromagnetic and ferrimagnetic ordering.[104] Extra counting times are often required since producing the polarized beam necessarily reduces the flux.

Designs through coordination chemistry have led to low-dimensional magnetic systems by suitable control of the 3D crystal structure to include well isolated one-dimensional (1D) chains or two-dimensional (2D) layers.[110a] The further introduction and control of high magnetic anisotropy or multiferroicity, for example, can then lead to potentially useful applied physical properties. A series of such chiral, polar topological ferrimagnets have been investigated on HB-2A (Figure 12). These compounds $M_3(OOCH)_5Cl(OH_2)$ [M = Fe(II), Co(II), Ni(II)] are composed of 1D chains that are twisted into helices.[110a] The magnetic structure was determined using variable-temperature (VT) neutron powder diffraction on HB-2A, indicating that the moments are aligned in the same direction as the polarity of the helical chains. The results suggest that these materials could be potential multiferroics.

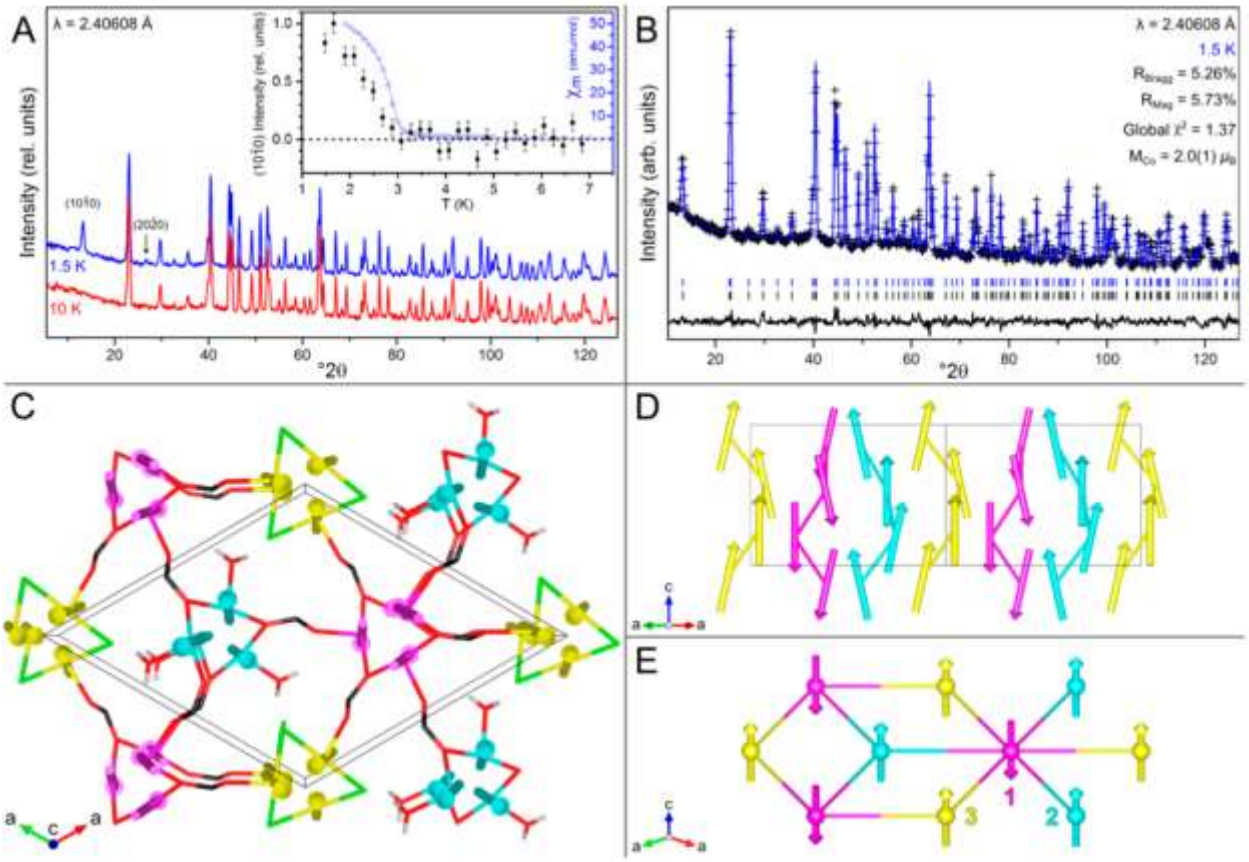

Figure 12. Neutron powder diffraction and magnetic structure of $Co_3(OOCH)_5Cl(OH_2)$ measured on HB-2A.[110a] (A) Diffraction patterns taken at 10 K and 1.5 K show additional magnetic reflections at 1.5 K. Inset: Order parameter for the $(1,0,\bar{1},0)$ reflection, compared to the temperature dependence of the magnetic susceptibility. (B) Rietveld refinement of the 1.5 K data. Tick marks show the nuclear (black) and magnetic (blue) reflections. Despite the high sloping background from the large hydrogen content the structural refinement and magnetic signal are well defined. (C) General view of the magnetic structure viewed along [0001] with intrachain formates and non-water hydrogens omitted for clarity. (D) Side view along $[11\bar{2}0]$ showing only the metal atoms. (E) Diagram showing the net magnetic moment of each chain and interchain connectivity. Reprint with permission by the American Chemical Society.

Powder diffraction instruments are prevalent in all the neutron sources in the world and tend to be workhorse instruments for structural characterization. In addition to POWGEN, most of the diffractometers at other spallation sources like ISIS in the UK and JPARC in Japan have more traditional design where multiple histograms are produced based on resolution focusing. Examples include HRPD,[111] GEM,[112] Polaris[113] and WISH[114] at ISIS (UK), SuperHRPD,[115] SPICA[116] and iMATERIA[117] at J-PARC (Japan). There are 3 powder diffractometers at ILL in France (D1B,[118] D2B[119] and D20[120]), two in Budapest Neutron Centre (PSD[121] and TOF-ND[122]), while the Australian reactor (ANSTO) is home for Echidna[123] and WOMBAT.[124] The instrument design and operation of BT-1 at NIST, HB-2A at HFIR, ORNL and D2B at ILL (France) are similar with a bank of separated ^{3}He detectors. They are also comparable to reactor-based diffractometers with position-sensitive detectors such as D20 at the ILL and ECHIDNA and WOMBAT at ANSTO (Australia). This is by no means an exhaustive list of neutron powder

diffractometers around the world but are some samplings of beamlines that have similar science portfolio as POWGEN, BT-1 and HB-2A.

4. Inelastic Neutron Scattering (INS) Spectrometers

Indirect-geometry INS spectrometer VISION[30a] is discussed first. Direct-geometry INS spectrometers to be presented next are CNCS,[25] DCS,[27] and SEQUOIA.[26] CNCS and DCS are similar in that both are cold neutron (i.e., low energy) spectrometers which are especially designed to probe small energy excitations. SEQUOIA, in comparison, is designed to probe larger energy excitations. MACS with characteristics of a triple-axis instrument is discussed last.

4.1. VISION at ORNL

Vibrational Spectrometer (VISION) is designed for neutron vibrational spectroscopy.[30a] It has also been used to probe magnetic transitions. The instrument dynamic range is ca. 0-8,000 cm^{-1} with resolution of ($\Delta E/E_i$ =) 1.5% of the incident neutron energy at >40 cm^{-1}. The analyzers are arranged in two groups for forward (low Q) and backward (high Q) scattering (Scheme 3-Right).

Vibrational spectroscopy is an analytical technique to probe molecular structures, chemical bonding, and intermolecular interactions. IR and Raman spectroscopies have been widely used to study molecular vibrations. VISION uses neutrons rather than photons to investigate molecular vibrations. As indicated earlier, this approach has several advantages over optical spectroscopies such as IR and Raman, including high sensitivity to hydrogen, absence of selection rules that govern IR and Raman spectroscopies, ease of computation of the vibrational spectrum, isotopic sensitivity, no energy deposition in sample, and high neutron penetrability

through bulky sample environment.[1d, 30b]

The science performed on VISION is diverse.[125] The spectrometer is particularly efficient at exploiting the large incoherent cross section of hydrogen atoms. Studies of hydrogenous materials are therefore a popular topic at VISION, including water in confinement, hydrogen bonding, hydrogen storage, basic organic chemistry, catalysis and surface chemistry, polymers, batteries and fuel cells, porous materials, hydrous minerals, complex hydrides, proton conductors, and ligand dynamics in organometallic compounds.[30b, 126] Non-hydrogenous materials are also studied thanks to the high neutron flux at SNS and the optimized instrument geometry. Neutrons exchange momentum with a sample. In view of the instrument configuration, the entire Brillouin zone of a solid is sampled during an experiment. The result is a density of states averaged over the Brillouin zone in contrast to optical spectrum, which produces a vibrational spectrum at the Γ point of the Brillouin zone only. The density of states thus obtained can be used in the evaluation of the lattice dynamics contribution to thermodynamic quantities such as entropy or specific heat.

The simplicity of the neutron-nucleus interaction permits the quantitative (mode frequencies and intensities) computation of the neutron vibrational spectrum with *ab initio* electronic structure methods. The output of these calculations can be directly and quantitatively compared to the experimental vibrational spectra.[127] This comparison is a far more stringent test of the validity of a computation or computational method than a comparison with the predicted structure. The phonon density of states (measured and calculated) is also the main ingredient needed in determining a number of thermodynamic properties. The scattering intensity measured with INS is proportional to the Vibrational Density of States (VDOS) of the solid, uniformly averaged over the first Brillouin zone. As users perform experiments of increasing complexity,

the use of computer simulation is becoming an integral part of the data analysis to enable and accelerate data interpretation and publication. VISION runs its own, dedicated, medium-size computer cluster for "on-the-fly" simulation of vibrational spectra with conventional DFT, MD (molecular dynamics), and post-DFT methods. This initiative, Virtual Experiments in Spectroscopy (VirtuES), funded by Laboratory Directed Research and Development program (LDRD project No. 7739), ORNL permits the timely analysis and interpretation of neutron data. In some cases, the simulations provide users with data interpretation in real time to guide an experiment in progress at the beam line.

The VISION sample environments continue to be developed to respond to user demand and reflect the diversity of the user base. The most commonly used sample environment has been the top-loading closed-cycle refrigerator (CCR). Other new sample environments have been developed to broaden capabilities. These are discussed below.

(a) *CCR*. 4 K cryocoolers allow users to cool samples, devices and/or equipment without the inconvenience and expense of liquid helium with two main advantages: rapid sample exchange while the refrigerator is operating and efficient cooling for non-conductive or irregularly shaped samples not easily clamped to a cold finger (e.g., powders, liquid solutions, etc.). The sample is inserted, via a long stick, into a nearly isothermal region of the gas column for cooling. Sample exchange by simply removing the sample rod, switching samples on the rod, and reinserting the rod into the cryostat. The entire sequence takes only a few minutes and is performed while the refrigerator is operating. VISION has sticks for high pressure gas cells, in-situ gas loading, high temperature, and optical and electrical access to samples.

(b) *Gas panel*. The compact design and simple operation of the gas panel make it easy to use, giving access to a variety of gases, dosing volumes, high vacuum (10^{-6} mbar), pressure/vacuum

gauges, and the Hot-Off Gas (HOG) system for safe venting. The gas manifold, rated to 200 bar of pressure, is used heavily for in-situ gas loading in experiments involving porous materials, surface chemistry or catalysis.

(c) *Ortho/parahydrogen converter*. The large scattering cross section associated with the ortho to para rotational transition in hydrogen is particularly useful to observe H_2 and its interaction with environment. Normal (room temperature) hydrogen is 25% para-H_2 and 75% ortho-H_2. Catalytic conversion to 100% para-H_2 is possible at <20 K. VISION has a compact ortho/para converter, a small pressure vessel containing Cr(II) oxide catalyst and cooled by a cold finger to 14 K, to provide para-H_2. This equipment is connected to the gas panel described above.

(d) *Piston cells*. The core of the pressure cell, with pressure up to 20 kbar, is a Cu-Be alloy surrounded by Al. This cell, approximately 1 mL in volume, operates at low to room temperatures.

(e) *Gas cells*. Cu-Be and Al cells, rated for use up to 7 kbar, are for H_2 and gases other H_2, respectively.

An example of the use of INS by VISION is studies of relationships between vibrational dynamics and H_2 release from $LiCa(AlH_4)_3$ (Figure 13), showing, e.g., softening of the external motion of $[AlH_4]^-$ as an initial stage of the H_2 release.[125h]

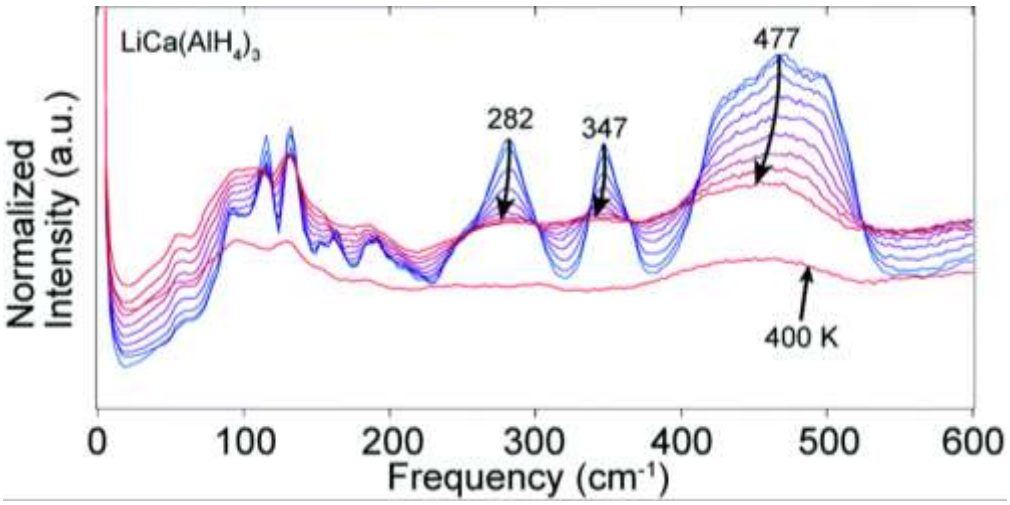

Figure 13. INS spectra of $LiCa(AlH_4)_3$ at 10–400 K.[125h] Reproduced from Ref. [125h] with permission from The Royal Society of Chemistry.

Simultaneous diffraction and inelastic scattering is not a reality at VISION yet but we expect this capability to develop and expand. While VISION exploits the large incoherent cross section of hydrogen atoms, powder neutron diffraction prefers the deuteration of hydrogenous samples. This reduces inelastic data collection rates so that simultaneous diffraction/inelastic scattering comes at a price.

VISION spectrometer can be compared with other indirect-geometry INS spectrometers TOSCA[128] at ISIS (UK), NERA[129] at FLNP (Russia), IN1-LAGRANGE[29] at ILL (France), and FANS[28b] at NIST (US). The last two use monochromatic incident neutron beam from a reactor (with variable E_i) and fixed energy of scattered neutrons ($E_f \approx 32$ cm^{-1}).

4.2. CNCS at ORNL

CNCS is a versatile, direct-geometry TOF spectrometer.[25, 130] It has 400 two meters long position sensitive detectors covering scattering angles from -50° to +135° in the scattering plane

and ±16° perpendicular to the scattering plane, that make it possible to map the 4-D scattering function $S(Q, \omega)$ in large portions of the reciprocal $\boldsymbol{Q}$ space and in the relevant energy-transfer range. CNCS uses a coupled cold H_2 moderator with a peak brightness at ~80 cm^{-1} neutron energy. The 35-m neutron guide has a horizontally curved central part which efficiently suppresses fast neutron background. The instrument provides both good energy ($\delta E/E$ = 1-3%) and momentum transfer resolution for inelastic and quasielastic neutron scattering experiments in the thermal and cold energy ranges (8-400 cm^{-1}). A large sample area allows hosting the wide range of sample environments to get (a) low and ultralow temperatures down to ~50 mK; (b) high temperatures ~1600 °C; (c) high magnetic fields up to 11 T; (d) high pressures up to 25 kbar. All of these, combined with the most powerful pulsed neutron source in the world, make the spectrometer especially relevant to studying the scientific questions addressed by inorganic chemistry such as kinetics, energy-resolved quasi-elastic scattering, dynamic properties of energy storage materials, low energy excitations (magnetic and crystal lattice), molecular magnetism, and quantum criticality. High performance software packages exist to reduce and scientifically analyze the data.[131]

CNCS has been in operation since May 2009 with more than 150 peer-reviewed user publications to date.[25] A good example of the CNCS use in coordination/inorganic chemistry is the determination of zero-field splitting (ZFS) parameter *D* of non-deuterated metalloporphyrins Mn(TPP)Cl (discussed earlier in Figure 3),[6g] Fe(TPP)X [X = F, Cl (Figure 5),[6g] Br, and I],[6h] and Mn(TPP).[6g] INS spectra of Mn(TPP) are given in Figure 14. There is a significant debate regarding the strategy for the design and synthesis of single-ion magnets (SIMs).[132] To rationally design SIMs, key factors dictating the sign and magnitude of *D* values in metal complexes need to be identified. In these studies, INS data provided a rare, complete

determination of ZFS parameters in a non-deuterated metalloporphyrin series.[6g, h]

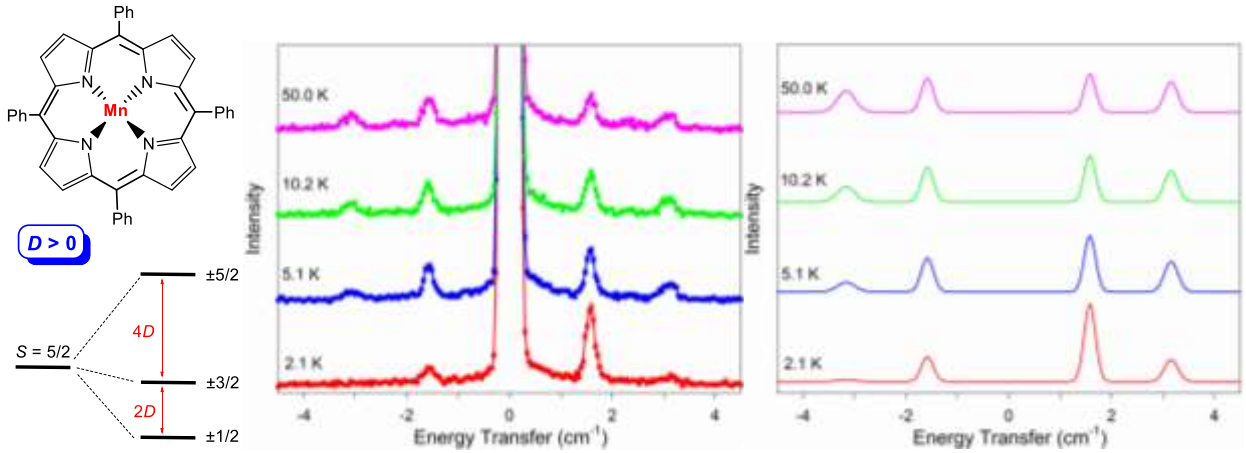

Figure 14. (Left) Mn(TPP) and its ZFS when its $D > 0$. (Middle) INS spectra of Mn(TPP). (Right) Calculated INS spectra of an $S = 5/2$ spin system with $D = 0.785$ cm^{-1}.[6g] Reprinted with permission by the American Chemical Society.

The instruments that provide low-incident neutron energies are widely used in many areas of solid and soft matter physics, chemistry and biology. Therefore, many pulsed as well as continuous neutron facilities around the world host similar instruments, such as IN5[133] at ILL (France), LET[134] at ISIS (UK), DCS at NIST (US) which is discussed below, TOFTOF at MLZ (Germany),[135] NEAT[136] at HZB (Germany), AMATERAS[137] at J-PARC (Japan), and . PELICAN at ANSTO (Australia).[138]

4.3. DCS at NIST

DCS is a pulsed TOF spectrometer on a guide emanating from the cold H_2 source out of the NIST reactor.[27, 139] An array of choppers define the wavelength, neutron packet size, and pulse rate onto the sample. The sample is in a large chamber that can accommodate both 10-T

and 11.5-T magnets covering temperature ranges from 50 mK to >300 K. The ^{3}He detectors cover scattering angles of -30^o to 140^o. Several parameters can be tuned so that the slowest neutrons from one pulse do not overlap with the fastest neutrons from a following pulse. Tools in the NIST free software package, DAVE,[140] allow one to quickly gauge the incident neutron intensity and resolution or fine tune the settings and see the effects on the *Q*-range, energy-transfer range, and elastic-resolution.

DCS is a versatile spectrometer that allows all suitable combinations of sample environment capabilities listed in Table 1 to be used along with the 11.5-T and 10-T magnets. The wide angular coverage makes it an excellent survey instrument when searching for low energy (around 8 cm^{-1}) magnetic or dynamic features in new materials. The excellent background makes it quite responsive even for very weak scattering systems, such as small moment magnetic fluctuations. For MOFs, it has been used to probe the dynamical response of jump-rotation of pyrazine rings in an inter-penetrated coordination framework,[141] identified the existence of a temperature induced 'breathing' for the pores in an MOF (MIL-53) through a change in low energy phonons,[83c] and detailed the orientation potential of the methyl groups in a zeolitic imidazolate framework (ZIF).[142]

While DCS-style instruments are excellent at determining diffusional time-scales and length-scales for adsorbed species,[143] there has been relatively few applications of DCS towards this goal in coordination polymer systems. Exceptions are the monitoring of the *Q* dependence of rotational lines for adsorbed H_2,[144] and the characterization of the liquid-like diffusion of the individual H_2 molecules in the pores of the MOFs Mg-MOF74[145] and MIL-53.[93a] On the atomic scale, the Grotthuss proton hopping mechanism in a new type of crystalline proton conductor composed of ammonium in a bridges zinc oxalate coordination polymer was

characterized.[146]

For molecular magnets[147] and low-dimensional magnetism of coordination polymers,[148] DCS has contributed extensively. Notably, it was used to illustrate that field dependent excitation energies agreed with the theory for the breather and soliton solutions to the quantum sine-Gordon model which is a proposed low energy theory for $S = 1/2$ chains in a staggered field measured at 40 mK and up to 11 T.[149] Aditional insights were gained from determination of the scaling relations of a Heisenberg $S = 1/2$ chain under 0 T and 7.5 T fields at 85 mK as established for a 2(1,4-dioxane)•2(H_2O)•$CuCl_2$ polymer by Zheludev et al.[150]

4.4. SEQUOIA at ORNL

SEQUOIA is also a direct-geometry TOF spectrometer with variable energies of incident neutrons from 32 to 16,000 cm^{-1}. The energies of incident neutrons are larger than those of CNCS or DCS.[151] Long sample-to-detector flight path (≥5.5 m) provides good wave-vector and energy resolution of ($\Delta E/E_i$ =) 1.5-5% at the elastic line and up to twice better at higher energy transfer. The entire secondary flight path of the spectrometer, from the sample to the detectors, is evacuated to a level of better than 10^{-6} mbar, resulting in low background data. The detector array covers -30° to 60° in the horizontal plane and ±18° in the vertical directions, thus providing a wide range of momentum transfer. The collected neutron scattering data are transformed from time-of-flight and instrument coordinates to the dynamical structure factor $S(Q,E)$. Therefore, the spectrometer can be successfully used for measurements of excitations having vibrational, tunneling, or magnetic origin. The INS experiments can be done on powder/polycrystalline and single-crystal samples. Measurements using powder/polycrystalline samples have revealed many important properties such as the density of the vibrational states,[152] tunneling,[153] and crystal

field splittings of the ground state.[154] Single-crystal samples have given the dispersion of the excitations in the crystal inverse space.[155]

One example is the use of INS by SEQUOIA to probe urea interaction within a titanium carbide-based MXene $Ti_3C_2T_z$ (T_z = termination group OH^-, F^-, or $O^{=}$).[152b] The 2-D materials MXenes may be intercalated for applications such as electrochemical energy storage, water purification, and sensing. The interactions between the intercalant, such as urea, and MXene itself, is, however, not well understood. INS has been used to study the interactions, revealing that urea is destabilized by 2-D materials to decompose to NH_4^+ cations which are intercalated in the MXenes. The Ti–urea complex, $Ti(urea)_6I_3$, and its INS spectra were used for comparison. One set of INS spectra are given in Figure 15, showing the regions dominated by NH_2 deformation and rocking modes and by the C–N stretching modes. Because of the high H neutron scattering cross section, the INS spectra are dominated by features involving H vibrations in the materials.[152b] In comparison, the neutron scattering cross sections of C and O atoms are small. Thus, the CO stretch near 1681 cm^{-1} is not observed (or it is buried in the shoulder of the much stronger NH_2 modes) in the INS spectra of urea [or 1636 cm^{-1} for $Ti(urea)_6I_3$], although this CO stretch is strong in the IR spectra of urea and $Ti(urea)_6I_3$. The 1460 and 1690 cm^{-1} peaks in u-MX and u-MX dried in Figure 15, which are not observed in the INS spectra of urea and $Ti(urea)_6I_3$, are assigned to the modes of NH_4^+ ions.[152b]

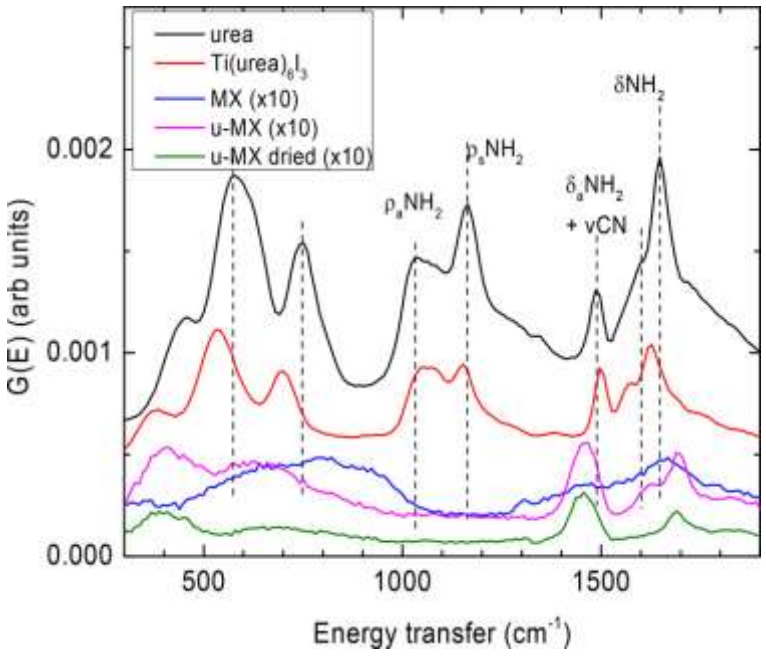

Figure 15. INS spectra of urea, $Ti(urea)_3I_3$, MX, u-MX and u-MX dried at 6 K (incident E_i = 2,016 cm^{-1}).[152b] Reprinted with permission by the American Chemical Society.

Instruments similar to SEQUOIA include ARCS[156] at SNS, ORNL, USA which has larger neutron flux and coarse energy resolution than SEQUOIA, HYSPEC[157] also at SNS which can do polarization analysis and uses $E_i < 484$ cm^{-1}, three spectrometers MERLIN,[158] MAPS[159] and MARI[160] in the UK, and 4SEASONS[161] in Japan which has lower energy resolution and $E_i < 2420$ cm^{-1}.

4.5. MACS at NIST

MACS is an instrument complementary to DCS in many ways but with characteristics of a triple-axis instrument.[31a] It is of particular use for studying fundamental interactions of spins in quantum materials and condensed matter systems. A further capability of interest to these

communities is the wide-angle polarization analysis capability.[162] The polarized flux is as high as 3×10^7 n/cm^2/s at ca. 30 cm^{-1} and 1×10^8 n/cm^2/s at 80 cm^{-1}.

Using both MACS and DCS, Hong et al., characterized the coupling in a two-leg spin ladder system which is an $S = 1/2$ quantum antiferromagnet with an ordering temperature of ca. 2 K, coexisting with a spin energy gap due to a small Ising anisotropy.[163] Further studies in crystals of (dimethylammonium)(3,5-dimethylpyridinium)$CuBr_4$ (DLCB) provided experimental evidence of field-induced spontaneous magnon decay.[164] The proposed 2D coupled two-leg ladder structure of DLCB is given in Figure 16-Left, showing the intraladder couplings J_{rung}, J_{leg} and interladder coupling J_{int}.[164] The two false-color maps of the background-subtracted spin-wave spectra in Figure 16-Right are examples of INS results in an external magnetic field from MACS, showing the observed spin gapped magnetic excitation spectra at 0 T and a renormalization of one-magnon dispersion at 4 T.

Further analysis of the spin Hamiltonian indicates that DLCB is close to a quantum critical point, and could exhibit a Higgs amplitude mode close in energy to the dominant transverse Nambu–Goldstone modes. Polarized inelastic neutron scattering measurements at MACS on 3.5 g of co-aligned single crystals allowed for the separation of the distribution of the longitudinal/Higgs amplitude modes compared to the transverse modes, a condensed matter physics analogy to the massless Higgs Boson.[165]

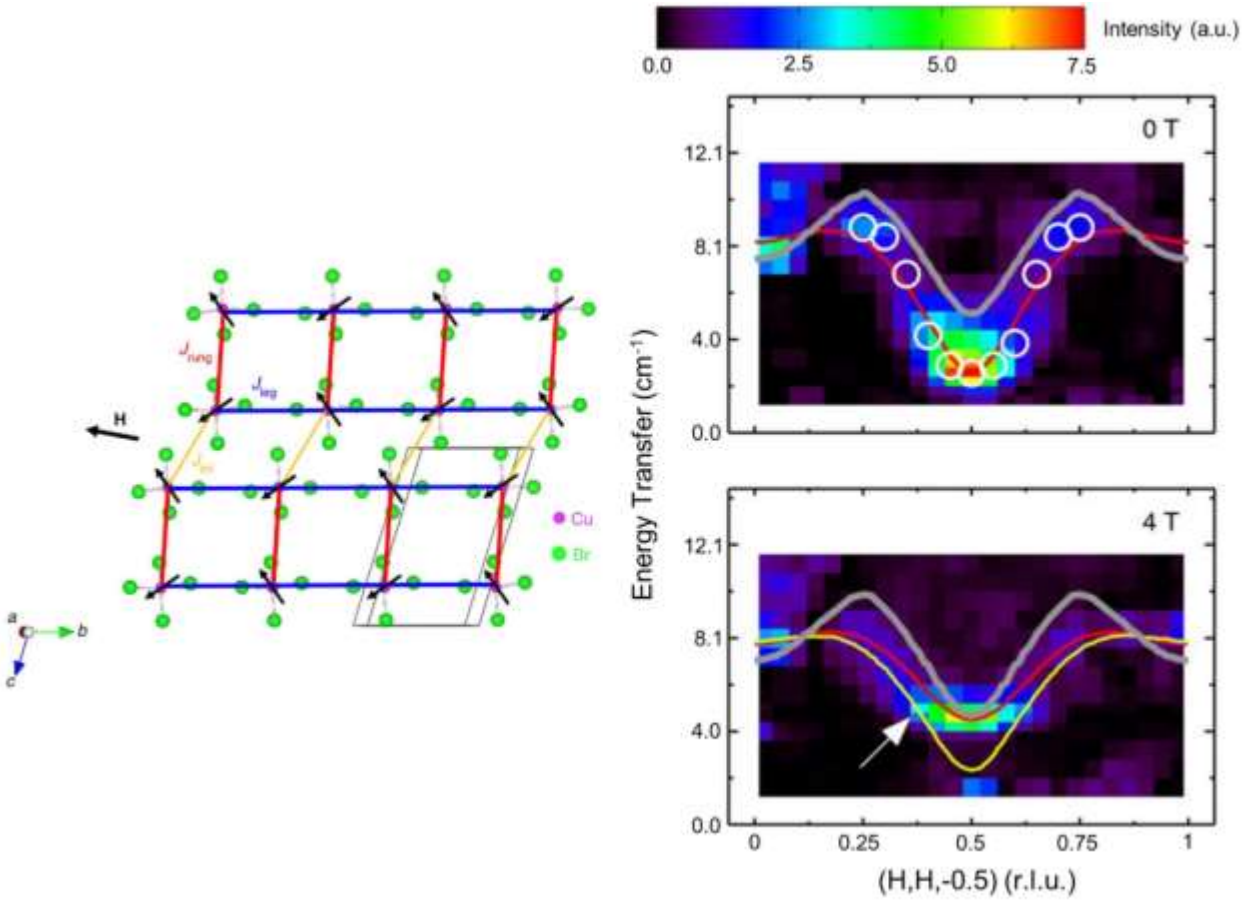

Figure 16. (Left) The proposed 2D coupled two-leg ladder structure of DLCB with the ladder chain extending along the *b* axis. Red, blue and orange lines indicate the intraladder couplings J_{rung}, J_{leg} and interladder coupling J_{int}, respectively. Black arrows indicate the canted spin structure in an external magnetic field applied along the [1 $\bar{1}$ 0] direction in the real space. (Right) Examples of INS results. False-color maps of the excitation spectra at 0 and 4 T as a function of energy and wave-vector transfer along the (H, H, −0.5) direction measured at T = 0.1 K. (r.l.u. = reciprocal lattice unit). Circle points represent the position of maximum intensity at each wave-vector. The white arrow indicates renormalization of the high-energy mode (TM_{high}). Red and yellow lines are the linear spin–wave theory calculations of the acoustic TM_{high} and TM_{low} (low-energy mode) one-magnon dispersion, respectively. Grey lines are the

calculated lower boundary of the two-magnon continuum.[164] Modified from the figures in Ref. [164]. Open access at https://www.nature.com/articles/ncomms15148#rightslink.

Triple-axis spectrometers are fairly common and are available in many neutron facilities. Since they are rarely used in the study of H-containing materials, the reader is encouraged to visit the websites of the neutron facilities if such needs arise.

5. Quasielastic Neutron Scattering (QENS) Spectrometers

There are two inverted-geometry backscattering spectrometers available to the user community in the USA. They have a similar operating principle, but different characteristics that makes them complementary to each other for many cases of studying complex dynamics that occur over many times scales, as shown below. Backscattering spectroscopy is based on the fact that the wavelength spread, $\delta\lambda$, of a Bragg-diffracted neutron beam decreases as the scattering angle, 2θ, approaches 180°. We will discuss some of the salient features of BASIS (ORNL)[166] and HFBS (NIST)[34] that indicate why one would choose either instrument and indicate the why they complement each other.

5.1. BASIS at ORNL

BASIS, neutron backscattering spectrometer at SNS, ORNL is the primary QENS-dedicated neutron spectrometer. The most distinguishing feature of BASIS[166] is its fine energy resolution (full width at half maximum of 0.03 cm^{-1} or better, depending on the sample dimensions). QENS signal of such width corresponds to the microscopic motions on ca. 0.4 ns time scale. At the same time, BASIS features a broad range of accessible neutron energy

transfers, from 0.8 cm^{-1} to 1.6 cm^{-1} to 4.0 cm^{-1}, depending on the chosen configuration, which translates into ca. 6 ps, 3 ps, and 1 ps, respectively. Thus, BASIS customarily probes microscopic motions on the ps to ns time scale, which are typically associated with diffusion- or relaxation-type dynamics. Because the momentum transfers accessible on BASIS (0.2 to 2.0 $Å^{-1}$) are commensurate with the inter-atomic and inter-molecular distances in condensed matter systems, the information on not only the temporal, but also the spatial, characteristics of the microscopic motions can be deduced from analysis of the momentum transfer dependence of the scattering signal. Such information is typically accessible only from molecular dynamics (MD) simulations, but not experimental techniques other than QENS. A combination of the fine energy resolution and a broad range of accessible energy transfers oftentimes allows simultaneous analysis of several dynamics components in the sample. As most samples studied at BASIS are hydrogen-bearing, the QENS signal from such samples is dominated by the strong incoherent scattering by H atoms, linked to single-particle, rather than inter-particle, motions. The neutron scattering cross-sections, either coherent or incoherent, for elements other than hydrogen are much smaller. This applies to deuterium as well. For this reason, partial deuteration of the sample can be used to make the deuterated species relatively “invisible” compared to their protonated counterparts. Many BASIS experiments involve QENS measurements at several chosen temperatures to make an Arrhenius plot of the dynamic parameters such as diffusivity or residence time between diffusion jump and obtain activation energies, besides the information on the geometry of the motions probed. Typical BASIS samples have a few millimoles of hydrogen. The lower limit is determined by the counting statistics required, whereas the upper limit is chosen to minimize the effects of neutron multiple scattering in the sample that could compromise the data quality. Thus, typical sample geometry is either of a thin annulus, or a thin

flat plate, approximately commensurate in size with the incident beam of 3 cm × 3 cm dimensions. With a few hours long measurements per a temperature point, a typical experiment on several samples might require a total of a few days.

BASIS has been employed in studies of diffusion- and relaxation-type dynamics in molecular metal oxide clusters. For example, the cluster with butyric acid $[Mo^{VI}_{72}Mo^{V}_{60}O_{372}(C_3H_7COO)_{24}(H_2O)_{84}]^{36-}$ as internal ligands, was selected as a representative model system to study the microscopic ligand dynamics.[167] The choice of such clusters was driven by (1) the bulkiness and close contact of ligands with neighboring molecules and (2) the presence of void space in the internal cluster area possibly suitable for encapsulation of guest molecules. The entering of guest molecules through the pores into the center void space of the clusters would be highly dependent on the ligands flexibility, which, in turn, is closely linked to their motions. Along with complementary INS measurements, QENS measurements have demonstrated that the cluster internal ligands are quite rigid, in contrast with the softness of regular alkyl tails in non-confined state. A cartoon of the motions, which can be quantified from QENS spectra measured at BASIS, is given in Figure 17-Left. Examples of the QENS spectra are given in Figure 17-Right. Such motions include $\langle u^2 \rangle$, mean-squared displacements of H atoms, a, spatial range of the translational motion of the C atom, and D_r, rotational diffusivity of methyl/methylene group. It was concluded that the stiffness of the cluster internal ligands can modify the encapsulation properties by displaying hard selection against the size of guest molecules, which has profound implications for catalytic properties of the clusters.

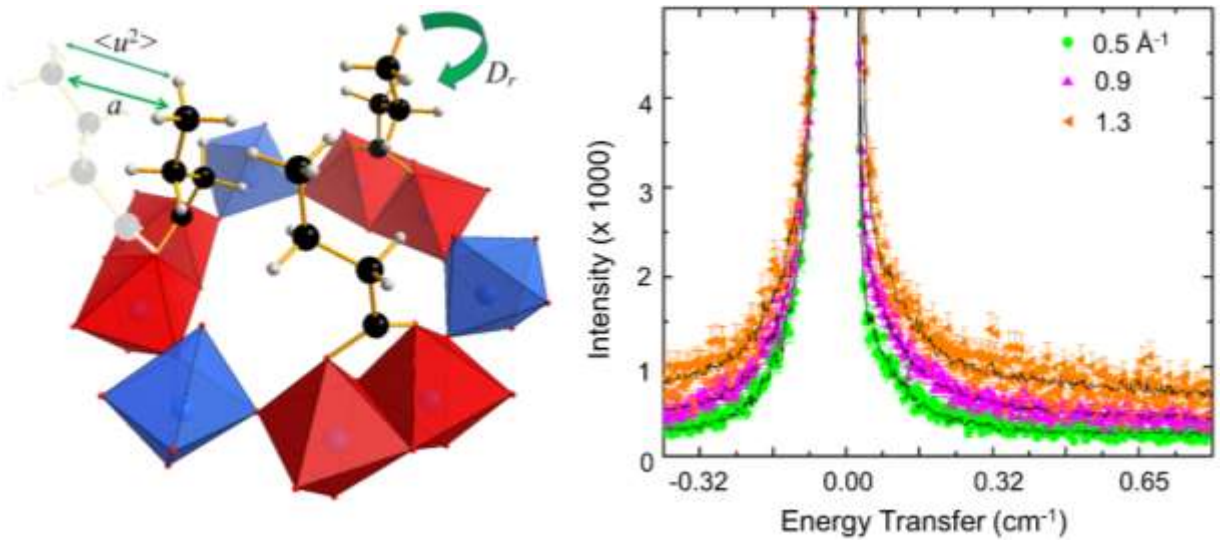

Figure 17. (Left) Important quantities in the QENS analysis of the cluster, including the displacement of the H atom in the time window of the QENS instrument and spatial range of the translational motion of the C atom. The cartoon shows how fast the rotational relaxation of the methyl or methylene group is.[167] (Right) QENS spectra of the cluster at 295 K.

In another study on BASIS, dynamics of water molecules in the internal space of gigantic core-shell polyoxometalates (POMs) was probed.[125g] Classic core-shell POMs ($Na_6[SiMo^{VI}_{12}O_{40}@Mo^{VI}_{68}Mo^{V}_{4}Fe^{III}_{30}O_{252}(CH_3CO_2)_{16}(H_2O)_{100}]$ were chosen for this study. Again, along with complementary INS experiments, QENS experiments have demonstrated that both structural and disordered water molecules are confined in the internal space between the core and the shell. Both types of water molecules play a vital role in the template synthetic reaction that produces POMs. In particular, they are responsible for centering of the cores and core-shell bridging, thereby leading to the stabilization of the core-shell structure. This finding is essential for development of applications of POMs in catalysis and as major building blocks in supramolecular science.

5.2. HFBS at NIST

HFBS is one of the highest intensity backscattering spectrometers using neutrons from a reactor source.[34] After diffracting from a Doppler-monochromator, the neutrons are scattered by the sample, backscattered by analyzers, pass back through the sample again, and finally arrive at the detectors. When preparing samples, care must be taken in adjusting the sample amount in the beam (3 cm × 3 cm) to account for the neutrons passing twice through the sample and increasing the probability of having multiple scattering events. The instrument can be run in two modes: (a) Stationary Doppler. The instrument records the intensity within the elastic resolution in this "fixed window mode"; (b) Doppler moving at one of several frequencies. This mode gives rise to a variable dynamic range that also alters the elastic resolution. The fixed window mode is ideal for parametric studies (usually as a function of temperature including mK, though other parameters are possible but not an external magnetic field). It essentially identifies the onset of any dynamics that removes intensity from the elastic line and gives insight into where dynamic transitions occur and the potential timescales that any QENS would be observable. This mode optimizes time spent in the dynamic mode on HFBS, and can indicate if the dynamics is likely to be too fast and whether a TOF spectrometer would possibly be a more appropriate spectrometer for the QENS measurements. The resolution of HFBS is the best in the USA, but with a restricted dynamic range compared to BASIS. At a dynamic range of ±0.242 cm^{-1}, the full-width at half-maximum resolution is 0.0075 cm^{-1}.

An example illustrating the range of capabilities of HFBS is the study of the interpenetrated coordination network $Mn(N(CN)_2)_2$.pyrazine, which is comprised of layers of almost square planar sheets of Mn-NCNCN-Mn linkages bridged by pyrazine ligands that are coordinated through nitrogen bonds to the Mn(II) centers. At low temperatures, the system is

antiferromagnetic, but at >220 K, the framework becomes dynamic while the analogous Cu(II) compound does not.[141] A further dynamic transition is evident at around 400 K (Figure 18). The dynamic scans between 250 K and 400 K are used to follow the *Q*-dependence of the QENS signal. This unambiguously shows that the pyrazines have an activation energy of 24 ± 2 kJ mol^{-1}, for performing 2-fold jumps which were the fastest recorded in a solid matrix. Correlation times obtained from the QENS widths varied from ca. 17 ns to 1.9 ± 1 ns upon increasing the temperature from 250 K to 400 K. An abrupt increase in timescale from 1.9 ns to 70 ps between 400 K and 425 K coincides with a phase transition at 408 K and requires a TOF instrument to measure.

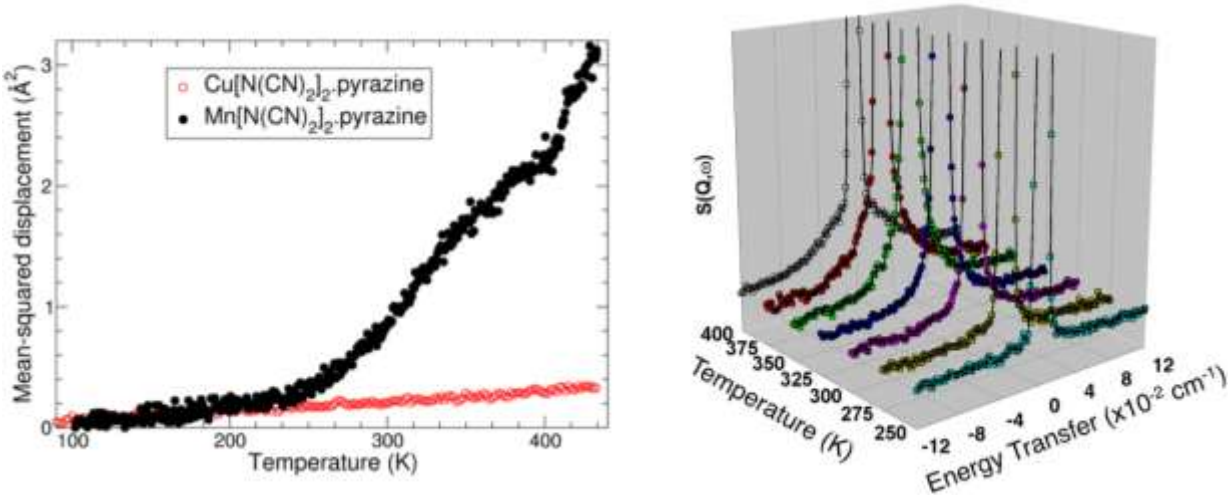

Figure 18. (Left) The dynamics of the H-containing pyrazine ligand in Mn[N(CN)2]2.pyrazine leads to an increase in the mean-squared displacement value over that of the more rigid Cu(II) polymorph. (Right) Temperature dependence of the scattering law for Mn[N(CN)2]2(pyrazine), emphasizing the growth of the QENS signal on HFBS. There is an increase in intensity of the quasielastic component as the temperature is raised to 400 K.[141] Reprinted with permission by the American Chemical Society.

Neutron backscattering spectrometers at facilities around the world include IN16B[168] at

ILL (France), IRIS[169] and OSIRIS[170] both at ISIS (UK), SPHERES[171] at MLZ (Germany), DNA[172] at J-PARC (Japan), and EMU[173] at ANSTO (Australia). In addition, direct-geometry TOF instruments are also capable of measuring QENS spectra in the ps-time scale.

It is the hope of the authors that this mini-review of neutron instruments relevant to research in coordination chemistry will help the reader to see potential use of the neutron scatterings in her/his own studies. In addition, with a list of the major instruments and their websites in one review, it would be easier for the reader to quickly find a particular instrument for the studies. With the expansion of the number of neutron instruments and the intense neutron flux provided by the spallation facilities such as SNS, China Spallation Neutron Source, and European Spallation Source under construction, more people are expected to use the unique features of neutron scatterings in their research.

Author Contributions

Z-L.X. proposed the writing of this mini-review. He and A.J.-R.C. organized the preparation of the mini-review. The following authors contributed to the sections in parentheses: C.M.B. (BT-1, DCS, MACS, and HFBS), S.C. (POWDER or HB-2A), H.B.C. and B.C.C. (FCD or HB-3A), L.L.D. (VSION), A.H. (POWGEN), A.I.K. (SEQUOIA), E.M. (BASIS), A.A.P. (CNCS), and X.P.W. (TOPAZ). All authors have given approval to the final version of the manuscript.

Acknowledgment

The authors thank financial support by the US National Science Foundation (CHE-

1633870 to Z-L.X.). Acknowledgment is also made to the Donors of the American Chemical Society Petroleum Research Fund for partial support of this work. The research at ORNL's Spallation Neutron Source and High Flux Isotope Reactor was sponsored by the Scientific User Facilities Division, Office of Basic Energy Sciences, U.S. Department of Energy. The computing and software resources were made available through the VirtuES: Virtual Experiments in Spectroscopy (LDRD 7739) and the ICE-MAN: Integrated Computational Environment, Modeling and Analysis of Neutron data (LDRD 8237) projects, funded by the Laboratory Directed Research and Development program at ORNL. The authors thank Dr. Shelby E. Stavretis for making Scheme 3.

References

[1] a) G. E. Bacon, *Neutron Scattering in Chemistry*, Butterworth, London, **1977**; b) L. Pusztai in *Neutron Scattering Methods in Chemistry*, Eds.: A. Vertes, S. Nagy, Z. Klencsar, R. G. Lovas and F. Rosch), Springer, **2011**, pp. 1515-1551; c) C. C. Wilson, *Single Crystal Neutron Diffraction from Molecular Materials*, World Scientific, Singapore, **2000**; d) P. C. H. Mitchell, S. F. Parker, A. J. Ramirez-Cuesta and J. Tomkinson, *Vibrational Spectroscopy with Neutrons: With Applications in Chemistry, Biology, Materials Science and Catalysis*, World Scientific Publishing Company, **2005**, pp. 552-558; e) D. Gatteschi, *J. Phys. Chem. B* **2000**, *104*, 9780-9787; f) F. E. Fernandez-Alonso and D. L. E. Price, *Neutron Scattering - Fundamental*, Elsevier, **2013**; g) T. Chatterji, *Neutron Scattering from Magnetic Materials*, Elsevier, **2006**; h) D. L. E. Price and F. E. Fernandez-Alonso, *Neutron Scattering - Magnetic and Quantum Phenomena*, Elsevier, **2015**; i) F. E. Fernandez-Alonso and D. L. E. Price, *Neutron Scattering – Applications in Biology,*

Chemistry, and Materials Science, Elsevier, **2017**; j) J. M. Carpenter and C.-K. Loong, *Elements of Slow-Neutron Scattering: Basics, Techniques, and Applications*, Cambridge University Press, **2015**.

[2] SNS in *website: https://neutrons.ornl.gov/sns*.

[3] HFIR in *website: https://neutrons.ornl.gov/hfir*.

[4] NIST Center for Neutron Research in *website: https://www.nist.gov/ncnr*.

[5] a) G. L. Squires, *Introduction to the Theory of Thermal Neutron Scattering*, Cambridge University Press, **1978**, p; b) A. Furrer, J. Mesot and T. Strässle, *Neutron Scattering in Condensed Matter Physics*, World Scientific, **2009**.

[6] a) H. Andres, R. Basler, H.-U. Güdel, G. Aromí, G. Christou, H. Büttner and B. Rufflé, *J. Am. Chem. Soc.* **2000**, *122*, 12469-12477; b) R. Basler, A. Sieber, G. Chaboussant, H. U. Güdel, N. E. Chakov, M. Soler, G. Christou, A. Desmedt and R. Lechner, *Inorg. Chem.* **2005**, *44*, 649-653; c) S. Piligkos, G. Rajaraman, M. Soler, N. Kirchner, J. van Slageren, R. Bircher, S. Parsons, H.-U. Güdel, J. Kortus, W. Wernsdorfer, G. Christou and E. K. Brechin, *J. Am. Chem. Soc.* **2005**, *127*, 5572-5580; d) O. Waldmann, C. Dobe, H. Mutka, A. Furrer and H. U. Güdel, *Phys. Rev. Lett.* **2005**, *95*, 057202; e) A. B. Blake, C. E. Anson, S. K. arapKoske, R. D. Cannon, U. A. Jayasooriya, A. K. Saad, R. P. White and D. Summerfield, *J. Chem. Soc., Dalton Trans.* **1997**, 2039-2044; f) C. H. Wang, M. D. Lumsden, R. S. Fishman, G. Ehlers, T. Hong, W. Tian, H. Cao, A. Podlesnyak, C. Dunmars, J. A. Schlueter, J. L. Manson and A. D. Christianson, *Phys. Rev. B* **2012**, *86*, 064439; g) S. C. Hunter, A. A. Podlesnyak and Z.-L. Xue, *Inorg. Chem.* **2014**, *53*, 1955-1961; h) S. E. Stavretis, M. Atanasov, A. A. Podlesnyak, S. C. Hunter, F. Neese and Z.-L. Xue, *Inorg. Chem.* **2015**, *54*, 9790-9801; i) L. Chen, H.-H. Cui, S. E. Stavretis, S. C.

Hunter, Y.-Q. Zhang, X.-T. Chen, Y.-C. Sun, Z. Wang, Y. Song, A. A. Podlesnyak, Z.-W. Ouyang and Z.-L. Xue, *Inorg. Chem.* **2016**, *55*, 12603-12617.

[7] B. A. Dougan and Z. Xue, *Sci. China B Chem.* **2009**, *52*, 2083-2095.

[8] W. Guan, E. Wakai, T. Naoe, H. Kogawa, T. Wakui, K. Haga, H. Takada and M. Futakawa, *Nucl. Instr. Meth. Phys. Res. A* **2018**, *894*, 8-19.

[9] D. Wilcox, P. Loveridge, T. Davenne, L. Jones and D. Jenkins, *J. Nucl. Mater.* **2018**, *506*, 76-82.

[10] PSI in *website: https://www.psi.ch/sinq/the-neutron-source*.

[11] ISIS in *website: http://pd.chem.ucl.ac.uk/pdnn/inst3/pulsed.htm*.

[12] High-flux reactor at ILL in *website: https://www.ill.eu/reactor-and-safety/high-flux-reactor/*.

[13] FRM-II in *reactor website: https://www.frm2.tum.de/en/the-neutron-source/*.

[14] Budapest in *Research Reactor website: http://www.bnc.hu/?q=node/6*.

[15] OPAL in *website: http://www.ansto.gov.au/ResearchHub/OurInfrastructure/ACNS/Facilities/OPALReactor/index.htm*.

[16] V. L. Aksenov, *Physica B Condens. Matter.* **1991**, *174*, 438-442.

[17] M. Harada, M. Teshigawara, M. Ohi, E. Klinkby, L. Zanini, K. Batkov, K. Oikawa, Y. Toh, A. Kimura and Y. Ikeda, *Nucl. Instrum. Methods Phys. Res. A* **2018**, *903*, 38-45.

[18] a) CSNS in *website: http://english.ihep.cas.cn/csns/doc/1959.html*; b) W. Ni, H. Jing, L. Zhang and L. Ou, *Radiat. Phys. Chem.* **2018**, *152*, 43-48; c) L. Y. Zhang, H. T. Jing, J. Y. Tang, Q. Li, X. C. Ruan, J. Ren, C. J. Ning, Y. J. Yu, Z. X. Tan, P. C. Wang, Y. C. He and X. Q. Wang, *Appl. Radiat. Isot.* **2018**, *132*, 212-221.

[19] SINQ in *website:* https://www.psi.ch/sinq/.

[20] ESS in *website:* https://europeanspallationsource.se/.

[21] A. J. Schultz, M. R. V. Jorgensen, X. Wang, R. L. Mikkelson, D. J. Mikkelson, V. E. Lynch, P. F. Peterson, M. L. Green and C. M. Hoffmann, *J. Appl. Cryst.* **2014**, *47*, 915-921.

[22] D3 in *website:* https://www.ill.eu/users/instruments/instruments-list/d3/description/instrument-layout/.

[23] B. Gillon, C. Sangregorio, A. Caneschi, D. Gatteschi, R. Sessoli, E. Ressouche and Y. Pontillon, *Inorg. Chim. Acta* **2007**, *360*, 3802-3806.

[24] C. C. Wilson, P. F. Henry, M. Schmidtmann, V. P. Ting, E. Williams and M. T. Weller, *Crystallog. Rev.* **2014**, *20*, 162-206.

[25] CNCS in *website:* https://neutrons.ornl.gov/cncs.

[26] SEQUOIA in *website:* https://neutrons.ornl.gov/sequoia.

[27] J. R. D. Copley and J. C. Cook, *Chem. Phys.* **2003**, *292*, 477-485.

[28] a) T. J. Udovic, D. A. Neumann, J. Leão and C. M. Brown, *Nucl. Instr. Meth. Phys. Res. A* **2004**, *517*, 189-201; b) FANS in *website:* https://ncnr.nist.gov/instruments/fans/fans_princ.html.

[29] a) IN1 in *website:* https://www.ill.eu/en/users/instruments/instruments-list/in1-taslagrange/description/instrument-layout/; b) I. Alexandre, J.-R. Mónica and K. Jiri, *J. Phys. Conf. Ser.* **2014**, *554*, 012001.

[30] a) P. A. Seeger, L. L. Daemen and J. Z. Larese, *Nucl. Instr. Meth. Phys. Res. A* **2009**, *604*, 719-728; b) S. F. Parker, A. J. Ramirez-Cuesta and L. Daemen, *Spectrochim. Acta A* **2018**, *190*, 518-523.

[31] a) J. A. Rodriguez, D. M. Adler, P. C. Brand, C. Broholm, J. C. Cook, C. Brocker, R. Hammond, Z. Huang, P. Hundertmark, J. W. Lynn, N. C. Maliszewskyj, J. Moyer, J. Orndorff, D. Pierce, T. D. Pike, G. Scharfstein, S. A. Smee and R. Vilaseca, *Meas. Sci. Technol.* **2008**, *19*, 034023; b) MACS in *website:* https://ncnr.nist.gov/instruments/macs/.

[32] a) B. Frick in *Neutron Backscattering Spectroscopy*, Eds.: F. Hippert, E. Geissler, J. L. Hodeau, E. Lelièvre-Berna and J.-R. Regnard), Springer, Dordrecht, **2006**, pp. 483-527; b) M. Bée, *Quasielastic Neutron Scattering. Principles and Applications in Solid State Chemistry, Biology and Materials Science*, Adam Hilger, Bristol, U.K., **1988**.

[33] M. Kofu, T. Kajiwara, J. S. Gardner, G. G. Simeoni, M. Tyagi, A. Faraone, K. Nakajima, S. Ohira-Kawamura, M. Nakano and O. Yamamuro, *Chem. Phys.* **2013**, *427*, 147-152.

[34] HFBS in *website:* https://ncnr.nist.gov/instruments/hfbs/.

[35] S. E. Stavretis, E. Mamontov, D. H. Moseley, Y. Cheng, L. L. Daemen, A. J. Ramirez-Cuesta and Z.-L. Xue, *Phys. Chem. Chem. Phys.* **2018**, *20*, 21119-21126.

[36] TOPAZ in *website:* https://neutrons.ornl.gov/topaz.

[37] a) HB-3A in *website:* https://neutrons.ornl.gov/hb3a; b) B. C. Chakoumakos, H. Cao, F. Ye, A. D. Stoica, M. Popovici, M. Sundaram, W. Zhou, J. S. Hicks, G. W. Lynn and R. A. Riedel, *J. Appl. Cryst.* **2011**, *44*, 655-658.

[38] C. M. Lieberman, M. C. Barry, Z. Wei, A. Y. Rogachev, X. Wang, J.-L. Liu, R. Clerac, Y.-S. Chen, A. S. Filatov and E. V. Dikarev, *Inorg. Chem.* **2017**, *56*, 9574-9584.

[39] Y. Ren, I. W. H. Oswald, X. Wang, G. T. McCandless and J. Y. Chan, *Cryst Growth Des.* **2016**, *16*, 2945-2951.

[40] M. Dembowski, T. A. Olds, K. L. Pellegrini, C. Hoffmann, X. P. Wang, S. Hickam, J. H. He, A. G. Oliver and P. C. Burns, *J. Am. Chem. Soc.* **2016**, *138*, 8547-8553.

[41] H. Xu, C. T. Hu, X. Wang and T. Diao, *Organometallics* **2017**, *36*, 4099-4102.

[42] a) A. S. Pandey, T. V. Harris, L. J. Giles, J. W. Peters and R. K. Szilagyi, *J. Am. Chem. Soc.* **2008**, *130*, 4533-4540; b) G. Berggren, A. Adamska, C. Lambertz, T. R. Simmons, J. Esselborn, M. Atta, S. Gambarelli, J. M. Mouesca, E. Reijerse, W. Lubitz, T. Happe, V. Artero and M. Fontecave, *Nature* **2013**, *499*, 66-69.

[43] T. B. Liu, D. L. DuBois and R. M. Bullock, *Nat. Chem.* **2013**, *5*, 228-233.

[44] T. Liu, X. Wang, C. Hoffmann, D. L. DuBois and R. M. Bullock, *Angew. Chem.* **2014**, *126*, 5440-5444; *Angew. Chem. Int. Ed.* **2014**, *53*, 5300-5304.

[45] R. S. Dhayal, J.-H. Liao, S. Kahlal, X. Wang, Y.-C. Liu, M.-H. Chiang, W. E. van Zyl, J.-Y. Saillard and C. W. Liu, *Chem. Eur. J* **2015**, *21*, 8369-8374.

[46] R. S. Dhayal, J.-H. Liao, X. Wang, Y.-C. Liu, M.-H. Chiang, S. Kahlal, J.-Y. Saillard and C. W. Liu, *Angew. Chem.* **2015**, *127*, 13808-13812; *Angew. Chem. Int. Ed.* **2015**, *54*, 13604-13608.

[47] J.-H. Liao, R. S. Dhayal, X. Wang, S. Kahlal, J.-Y. Saillard and C. W. Liu, *Inorg. Chem.* **2014**, *53*, 11140-11145.

[48] W. M. Potter, Y. Lai, H. Cao, R. E. Baumbach and S. E. Latturner, *Chem. Mater.* **2018**, *30*, 3806-3812.

[49] X. Ma, J. B. Whalen, H. Cao and S. E. Latturner, *Chem. Mater.* **2013**, *25*, 3363-3372.

[50] Y. Hu, C.-W. Chen, H. Cao, F. Makhmudov, J. H. Grebenkemper, M. N. Abdusalyamova, E. Morosan and S. M. Kauzlarich, *J. Am. Chem. Soc.* **2016**, *138*, 12422-12431.

[51] X. Tan, G. Fabbris, D. Haskel, A. A. Yaroslavtsev, H. Cao, C. M. Thompson, K. Kovnir, A. P. Menushenkov, R. V. Chernikov, V. O. Garlea and M. Shatruk, *J. Am. Chem. Soc.* **2016**, *138*, 2724-2731.

[52] a) H. B. Cao, Z. Y. Zhao, M. Lee, E. S. Choi, M. A. McGuire, B. C. Sales, H. D. Zhou, J.-Q. Yan and D. G. Mandrus, *APL Materials* **2015**, *3*, 062512; b) C. W. Li, J. Ma, H. B. Cao, A. F. May, D. L. Abernathy, G. Ehlers, C. Hoffmann, X. Wang, T. Hong, A. Huq, O. Gourdon and O. Delaire, *Phys. Rev. B* **2014**, *90*, 214303; c) H. Cao, B. C. Chakoumakos, X. Chen, J. Yan, M. A. McGuire, H. Yang, R. Custelcean, H. Zhou, D. J. Singh and D. Mandrus, *Phys. Rev. B* **2013**, *88*, 115122.

[53] SXD in *website:* *https://www.isis.stfc.ac.uk/Pages/SXD.aspx*.

[54] T. Ohhara, R. Kiyanagi, K. Oikawa, K. Kaneko, T. Kawasaki, I. Tamura, A. Nakao, T. Hanashima, K. Munakata, T. Moyoshi, T. Kuroda, H. Kimura, T. Sakakura, C. H. Lee, M. Takahashi, K. Ohshima, T. Kiyotani, Y. Noda and M. Arai, *J. Appl. Cryst.* **2016**, *49*, 120-127.

[55] FALCON in *website:* *https://www.helmholtz-berlin.de/pubbin/igama_output?modus=einzel&sprache=en&gid=1887&typoid=39942*.

[56] Koala in *website:* *https://www.ansto.gov.au/user-access/instruments/neutron-scattering-instruments/koala-laue-diffractometer*.

[57] a) VIVALDI in *website:* *https://www.ill.eu/users/scientific-groups/diffraction/instruments/*; b) C. Wilkinson, J. A. Cowan, D. A. A. Myles, F. Cipriani and G. J. McIntyre, *Neutron News* **2002**, *13*, 37-41.

[58] CORELLI in *website:* *https://neutrons.ornl.gov/corelli*.

[59] ManDi in *website:* *https://neutrons.ornl.gov/mandi*.

[60] SNAP in *website:* *https://neutrons.ornl.gov/snap*.

[61] D9 in *website:* *https://www.ill.eu/users/instruments/instruments-list/d9/description/instrument-layout/*.

[62] D10 in *website:* *https://www.ill.eu/users/instruments/instruments-list/d10/description/instrument-layout/*.

[63] HEiDi in *website:* *https://www.mlz-garching.de/heidi*.

[64] ZEBRA in *website:* *https://www.psi.ch/sinq/zebra/*.

[65] BL18 in *website:* *http://mlfuser.cross-tokai.jp/en/bl18.html*.

[66] POWGEN in *website:* *https://neutrons.ornl.gov/powgen*.

[67] BT-1 in *website:* *https://www.ncnr.nist.gov/instruments/bt1/*.

[68] a) HB-2A in *website:* *https://neutrons.ornl.gov/powder*; b) V. O. Garlea, B. C. Chakoumakos, S. A. Moore, G. B. Taylor, T. Chae, R. G. Maples, R. A. Riedel, G. W. Lynn and D. L. Selby, *Appl. Phys. A* **2010**, *99*, 531-535.

[69] G. Pawley, *J. Appl. Cryst.* **1981**, *14*, 357-361.

[70] A. Le Bail, *Powder Diffr.* **2005**, *20*, 316-326.

[71] H. Rietveld, *J. Appl. Cryst.* **1969**, *2*, 65-71.

[72] R. E. Dinnebier and S. J. L. Billinge, *Powder diffraction: theory and practice*, Royal Society of Chemistry, **2008**, p.

[73] B. H. Toby and R. B. Von Dreele, *J. Appl. Cryst.* **2013**, *46*, 544-549.

[74] J. Rodríguez-Carvajal, *Commission on powder diffraction (IUCr). Newsletter* **2001**, *26*, 12-19.

[75] A. Coelho, *J. Appl. Cryst.* **2018**, *51*, 210-218.

[76] A. Huq, J. P. Hodges, O. Gourdon and L. Heroux in *Powgen: A third-generation highresolution high-throughput powder diffraction instrument at the Spallation Neutron Source*, *Vol.* **2011**.

[77] a) D. W. Shin, C. A. Bridges, A. Huq, M. P. Paranthaman and A. Manthiram, *Chem. Mater.* **2012**, *24*, 3720-3731; b) J.-H. Kim, A. Huq, M. Chi, N. P. W. Pieczonka, E. Lee, C. A. Bridges, M. M. Tessema, A. Manthiram, K. A. Persson and B. R. Powell, *Chem. Mater.* **2014**, *26*, 4377-4386; c) J. Liu, A. Huq, Z. Moorhead-Rosenberg, A. Manthiram and K. Page, *Chem. Mater.* **2016**, *28*, 6817-6821.

[78] a) T. Thompson, J. Wolfenstine, J. L. Allen, M. Johannes, A. Huq, I. N. David and J. Sakamoto, *J. Mater. Chem. A* **2014**, *2*, 13431-13436; b) S. Mukhopadhyay, T. Thompson, J. Sakamoto, A. Huq, J. Wolfenstine, J. L. Allen, N. Bernstein, D. A. Stewart and M. D. Johannes, *Chem. Mater.* **2015**, *27*, 3658-3665; c) T. Thompson, A. Sharafi, M. D. Johannes, A. Huq, J. L. Allen, J. Wolfenstine and J. Sakamoto, *Adv. Energy Mater.* **2015**, *5*, 1500096.

[79] a) J. Adanez, A. Abad, F. Garcia-Labiano, P. Gayan and L. F. de Diego, *Prog. Energy Combust. Sci.* **2012**, *38*, 215-282; b) D. D. Taylor, N. J. Schreiber, B. D. Levitas, W. Xu, P. S. Whitfield and E. E. Rodriguez, *Chem. Mater.* **2016**, *28*, 3951-3960.

[80] J.-A. Dolyniuk, J. V. Zaikina, D. C. Kaseman, S. Sen and K. Kovnir, *Angew. Chem.* **2017**, *129*, 2458-2462; *Angew. Chem. Int. Ed.* **2017**, *56*, 2418-2422.

[81] J. R. D. Copley in *The Fundamentals of Neutron Powder Diffraction (NIST Recommended Practice Guide)*, *Vol.* **2001**.

[82] M. T. Weller, P. F. Henry, V. P. Ting and C. C. Wilson, *Chem. Commun.* **2009**, 2973-2989.

[83] a) H. Wu, T. Yildirim and W. Zhou, *J. Phys. Chem. Lett.* **2013**, *4*, 925-930; b) W. Zhou, H. Wu, T. Yildirim, J. R. Simpson and A. R. H. Walker, *Phys. Rev. B* **2008**, *78*, 054114; c) Y. Liu, J.-H. Her, A. Dailly, A. J. Ramirez-Cuesta, D. A. Neumann and C. M. Brown, *J. Am. Chem. Soc.* **2008**, *130*, 11813-11818; d) Q. Gao, J. Chen, Q. Sun, D. Chang, Q.

Huang, H. Wu, A. Sanson, R. Milazzo, H. Zhu, Q. Li, Z. Liu, J. Deng and X. Xing, *Angew. Chem.* **2017**, *129*, 9151-9156;
Angew. Chem. Int. Ed. **2017**, *56*, 9023-9028.

[84] H. Furukawa, F. Gándara, Y.-B. Zhang, J. Jiang, W. L. Queen, M. R. Hudson and O. M. Yaghi, *J. Am. Chem. Soc.* **2014**, *136*, 4369-4381.

[85] a) H. Wu, J. M. Simmons, G. Srinivas, W. Zhou and T. Yildirim, *J. Phys. Chem. Lett.* **2010**, *1*, 1946-1951; b) W. L. Queen, C. M. Brown, D. K. Britt, P. Zajdel, M. R. Hudson and O. M. Yaghi, *J. Phys. Chem. C* **2011**, *115*, 24915-24919; c) M. Asgari, S. Jawahery, E. D. Bloch, M. R. Hudson, R. Flacau, B. Vlaisavljevich, J. R. Long, C. M. Brown and W. L. Queen, *Chem. Sci.* **2018**, *9*, 4579-4588; d) M. Jiang, B. Li, X. Cui, Q. Yang, Z. Bao, Y. Yang, H. Wu, W. Zhou, B. Chen and H. Xing, *ACS Appl. Mater. Interfaces.* **2018**, *10*, 16628-16635.

[86] a) H. Wu, W. Zhou and T. Yildirim, *J. Am. Chem. Soc.* **2009**, *131*, 4995-5000; b) H. Wu, W. Zhou and T. Yildirim, *J. Phys. Chem. C* **2009**, *113*, 3029-3035; c) K. Lee, W. C. Isley, A. L. Dzubak, P. Verma, S. J. Stoneburner, L.-C. Lin, J. D. Howe, E. D. Bloch, D. A. Reed, M. R. Hudson, C. M. Brown, J. R. Long, J. B. Neaton, B. Smit, C. J. Cramer, D. G. Truhlar and L. Gagliardi, *J. Am. Chem. Soc.* **2014**, *136*, 698-704; d) B. Li, H.-M. Wen, H. Wang, H. Wu, M. Tyagi, T. Yildirim, W. Zhou and B. Chen, *J. Am. Chem. Soc.* **2014**, *136*, 6207-6210; e) B. Li, H.-M. Wen, H. Wang, H. Wu, T. Yildirim, W. Zhou and B. Chen, *Energ. Environ. Sci.* **2015**, *8*, 2504-2511; f) Z. Hulvey, B. Vlaisavljevich, J. A. Mason, E. Tsivion, T. P. Dougherty, E. D. Bloch, M. Head-Gordon, B. Smit, J. R. Long and C. M. Brown, *J. Am. Chem. Soc.* **2015**, *137*, 10816-10825.

[87] a) S. Xiang, W. Zhou, J. M. Gallegos, Y. Liu and B. Chen, *J. Am. Chem. Soc.* **2009**, *131*, 12415-12419; b) S. Xiang, W. Zhou, Z. Zhang, M. A. Green, Y. Liu and B. Chen, *Angew. Chem.* **2010**, *122*, 4719-4722; *Angew. Chem. Int. Ed.* **2010**, *49*, 4615-4618.

[88] Z. Hulvey, K. V. Lawler, Z. Qiao, J. Zhou, D. Fairen-Jimenez, R. Q. Snurr, S. V. Ushakov, A. Navrotsky, C. M. Brown and P. M. Forster, *J. Phys. Chem. C* **2013**, *117*, 20116-20126.

[89] Y. Tulchinsky, C. H. Hendon, K. A. Lomachenko, E. Borfecchia, B. C. Melot, M. R. Hudson, J. D. Tarver, M. D. Korzyński, A. W. Stubbs, J. J. Kagan, C. Lamberti, C. M. Brown and M. Dincă, *J. Am. Chem. Soc.* **2017**, *139*, 5992-5997.

[90] L. J. Murray, M. Dinca, J. Yano, S. Chavan, S. Bordiga, C. M. Brown and J. R. Long, *J. Am. Chem. Soc.* **2010**, *132*, 7856-7857.

[91] a) E. D. Bloch, L. J. Murray, W. L. Queen, S. Chavan, S. N. Maximoff, J. P. Bigi, R. Krishna, V. K. Peterson, F. Grandjean, G. J. Long, B. Smit, S. Bordiga, C. M. Brown and J. R. Long, *J. Am. Chem. Soc.* **2011**, *133*, 14814-14822; b) E. D. Bloch, M. R. Hudson, J. A. Mason, S. Chavan, V. Crocellà, J. D. Howe, K. Lee, A. L. Dzubak, W. L. Queen, J. M. Zadrozny, S. J. Geier, L.-C. Lin, L. Gagliardi, B. Smit, J. B. Neaton, S. Bordiga, C. M. Brown and J. R. Long, *J. Am. Chem. Soc.* **2014**, *136*, 10752-10761; c) P. Li, Y. He, Y. Zhao, L. Weng, H. Wang, R. Krishna, H. Wu, W. Zhou, M. O'Keeffe, Y. Han and B. Chen, *Angew. Chem.* **2015**, *127*, 584-587; *Angew. Chem. Int. Ed.* **2015**, *54*, 574-577; d) T.-L. Hu, H. Wang, B. Li, R. Krishna, H. Wu, W. Zhou, Y. Zhao, Y. Han, X. Wang, W. Zhu, Z. Yao, S. Xiang and B. Chen, *Nat. Commun.* **2015**, *6*, 7328; e) H. Wang, B. Li, H. Wu, T.-L. Hu, Z. Yao, W. Zhou, S. Xiang and B. Chen, *J. Am. Chem. Soc.* **2015**, *137*, 9963-9970; f) B. Li, X. Cui, D. O'Nolan, H.-M. Wen, M. Jiang, R. Krishna, H. Wu, R.-B.

Lin, Y.-S. Chen, D. Yuan, H. Xing, W. Zhou, Q. Ren, G. Qian, M. J. Zaworotko and B. Chen, *Adv. Mater.* **2017**, *29*, 1704210; g) L. Li, R.-B. Lin, R. Krishna, X. Wang, B. Li, H. Wu, J. Li, W. Zhou and B. Chen, *J. Mater. Chem. A* **2017**, *5*, 18984-18988; h) L. Li, R.-B. Lin, R. Krishna, X. Wang, B. Li, H. Wu, J. Li, W. Zhou and B. Chen, *J. Am. Chem. Soc.* **2017**, *139*, 7733-7736; i) R.-B. Lin, L. Li, H. Wu, H. Arman, B. Li, R.-G. Lin, W. Zhou and B. Chen, *J. Am. Chem. Soc.* **2017**, *139*, 8022-8028; j) G. R. Lorzing, B. A. Trump, C. M. Brown and E. D. Bloch, *Chem. Mater.* **2017**, *29*, 8583-8587; k) Z. Bao, D. Xie, G. Chang, H. Wu, L. Li, W. Zhou, H. Wang, Z. Zhang, H. Xing, Q. Yang, M. J. Zaworotko, Q. Ren and B. Chen, *J. Am. Chem. Soc.* **2018**, *140*, 4596-4603; l) E. J. Gosselin, G. R. Lorzing, B. A. Trump, C. M. Brown and E. D. Bloch, *Chem. Commun.* **2018**, *54*, 6392-6395.

[92] T. Yildirim and M. R. Hartman, *Phys. Rev. Lett.* **2005**, *95*, 215504.

[93] a) R. A. Pollock, J.-H. Her, C. M. Brown, Y. Liu and A. Dailly, *J. Phys. Chem. C* **2014**, *118*, 18197-18206; b) H. Wu, W. Zhou and T. Yildirim, *J. Am. Chem. Soc.* **2007**, *129*, 5314-5315.

[94] a) M. Dincă, A. Dailly, Y. Liu, C. M. Brown, D. A. Neumann and J. R. Long, *J. Am. Chem. Soc.* **2006**, *128*, 16876-16883; b) M. R. Hartman, V. K. Peterson, Y. Liu, S. S. Kaye and J. R. Long, *Chem. Mater.* **2006**, *18*, 3221-3224; c) V. K. Peterson, Y. Liu, C. M. Brown and C. J. Kepert, *J. Am. Chem. Soc.* **2006**, *128*, 15578-15579; d) M. Dincă, W. S. Han, Y. Liu, A. Dailly, C. M. Brown and J. R. Long, *Angew. Chem.* **2007**, *119*, 1441-1444; *Angew. Chem. Int. Ed.* **2007**, *46*, 1419-1422; e) D. Gygi, E. D. Bloch, J. A. Mason, M. R. Hudson, M. I. Gonzalez, R. L. Siegelman, T. A. Darwish, W. L. Queen, C. M. Brown and J. R. Long, *Chem. Mater.* **2016**, *28*, 1128-1138; f) C. M. Brown, A. J. Ramirez-Cuesta,

J.-H. Her, P. S. Wheatley and R. E. Morris, *Chem. Phys.* **2013**, *427*, 3-8; g) K. Sumida, J.-H. Her, M. Dincă, L. J. Murray, J. M. Schloss, C. J. Pierce, B. A. Thompson, S. A. FitzGerald, C. M. Brown and J. R. Long, *J. Phys. Chem. C* **2011**, *115*, 8414-8421; h) J. Luo, H. Xu, Y. Liu, Y. Zhao, L. L. Daemen, C. Brown, T. V. Timofeeva, S. Ma and H.-C. Zhou, *J. Am. Chem. Soc.* **2008**, *130*, 9626-9627; i) X. Lin, I. Telepeni, A. J. Blake, A. Dailly, C. M. Brown, J. M. Simmons, M. Zoppi, G. S. Walker, K. M. Thomas, T. J. Mays, P. Hubberstey, N. R. Champness and M. Schröder, *J. Am. Chem. Soc.* **2009**, *131*, 2159-2171; j) V. K. Peterson, C. M. Brown, Y. Liu and C. J. Kepert, *J. Phys. Chem. C* **2011**, *115*, 8851-8857.

[95] M. T. Kapelewski, S. J. Geier, M. R. Hudson, D. Stück, J. A. Mason, J. N. Nelson, D. J. Xiao, Z. Hulvey, E. Gilmour, S. A. FitzGerald, M. Head-Gordon, C. M. Brown and J. R. Long, *J. Am. Chem. Soc.* **2014**, *136*, 12119-12129.

[96] Y. Liu, H. Kabbour, C. M. Brown, D. A. Neumann and C. C. Ahn, *Langmuir* **2008**, *24*, 4772-4777.

[97] T. Runčevski, M. T. Kapelewski, R. M. Torres-Gavosto, J. D. Tarver, C. M. Brown and J. R. Long, *Chem. Commun.* **2016**, *52*, 8251-8254.

[98] C. G. Shull and J. S. Smart, *Phys. Rev.* **1949**, *76*, 1256-1257.

[99] a) J. L. Manson, Q.-z. Huang, C. M. Brown, J. W. Lynn, M. B. Stone, J. Singleton and F. Xiao, *Inorg. Chem.* **2015**, *54*, 11897-11905; b) C. R. Kmety, Q. Huang, J. W. Lynn, R. W. Erwin, J. L. Manson, S. McCall, J. E. Crow, K. L. Stevenson, J. S. Miller and A. J. Epstein, *Phys. Rev. B* **2000**, *62*, 5576-5588; c) J. L. Manson, Q.-z. Huang, J. W. Lynn, H.-J. Koo, M.-H. Whangbo, R. Bateman, T. Otsuka, N. Wada, D. N. Argyriou and J. S. Miller, *J. Am. Chem. Soc.* **2001**, *123*, 162-172; d) J. L. Manson, C. M. Brown, Q. Huang,

J. A. Schlueter, T. Lancaster, S. J. Blundell, J. Singleton, J. W. Lynn and F. L. Pratt, *Polyhedron* **2013**, *52*, 679-688.

[100] J. W. Lynn, Y. Chen, S. Chang, Y. Zhao, S. Chi, W. Ratcliff, B. G. Ueland and R. W. Erwin, *J. Res. Natl. Inst. Stand. Technol.* **2012**, *117*, 61-79.

[101] C.-H. Lee, C.-W. Wang, Y. Zhao, W.-H. Li, J. W. Lynn, A. B. Harris, K. Rule, H.-D. Yang and H. Berger, *Sci. Rep.* **2017**, *7*, 6437.

[102] J. Zhao, Q. Huang, C. de la Cruz, S. Li, J. W. Lynn, Y. Chen, M. A. Green, G. F. Chen, G. Li, Z. Li, J. L. Luo, N. L. Wang and P. Dai, *Nat. Mater.* **2008**, *7*, 953.

[103] Z. W. Ouyang, F. W. Wang, Q. Huang, W. F. Liu, Y. G. Xiao, J. W. Lynn, J. K. Liang and G. H. Rao, *Phys. Rev. B* **2005**, *71*, 064405.

[104] E. Lelièvre-Berna, A. S. Wills, E. Bourgeat-Lami, A. Dee, T. Hansen, P. F. Henry, A. Poole, M. Thomas, X. Tonon, J. Torregrossa, K. H. Andersen, F. Bordenave, D. Jullien, P. Mouveau, B. Guérard and G. Manzin, *Meas. Sci. Technol.* **2010**, *21*, 055106.

[105] L. Poudel, A. F. May, M. R. Koehler, M. A. McGuire, S. Mukhopadhyay, S. Calder, R. E. Baumbach, R. Mukherjee, D. Sapkota, C. de la Cruz, D. J. Singh, D. Mandrus and A. D. Christianson, *Phys. Rev. Lett.* **2016**, *117*, 235701.

[106] a) L. Zhou, J. Dai, Y. Chai, H. Zhang, S. Dong, H. Cao, S. Calder, Y. Yin, X. Wang, X. Shen, Z. Liu, T. Saito, Y. Shimakawa, H. Hojo, Y. Ikuhara, M. Azuma, Z. Hu, Y. Sun, C. Jin and Y. Long, *Adv. Mater.* **2017**, *29*, 1703435; b) X. Wang, Y. Chai, L. Zhou, H. Cao, C.-d. Cruz, J. Yang, J. Dai, Y. Yin, Z. Yuan, S. Zhang, R. Yu, M. Azuma, Y. Shimakawa, H. Zhang, S. Dong, Y. Sun, C. Jin and Y. Long, *Phys. Rev. Lett.* **2015**, *115*, 087601; c) T. Ferreira, G. Morrison, W. M. Chance, S. Calder, M. D. Smith and H.-C. zur Loye, *Chem. Mater.* **2017**, *29*, 2689-2693.

[107] a) M. A. McGuire, J. Yan, P. Lampen-Kelley, A. F. May, V. R. Cooper, L. Lindsay, A. Puretzky, L. Liang, S. Kc, E. Cakmak, S. Calder and B. C. Sales, *Phys. Rev. Mater.* **2017**, *1*, 064001; b) A. F. May, S. Calder, C. Cantoni, H. Cao and M. A. McGuire, *Phys. Rev. B* **2016**, *93*, 014411.

[108] a) S. Calder, J. G. Vale, N. A. Bogdanov, X. Liu, C. Donnerer, M. H. Upton, D. Casa, A. H. Said, M. D. Lumsden, Z. Zhao, J. Q. Yan, D. Mandrus, S. Nishimoto, J. van den Brink, J. P. Hill, D. F. McMorrow and A. D. Christianson, *Nat. Commun.* **2016**, *7*, 11651; b) S. Calder, D. J. Singh, V. O. Garlea, M. D. Lumsden, Y. G. Shi, K. Yamaura and A. D. Christianson, *Phys. Rev. B* **2017**, *96*, 184426.

[109] J. Mao, J. Shuai, S. Song, Y. Wu, R. Dally, J. Zhou, Z. Liu, J. Sun, Q. Zhang, C. dela Cruz, S. Wilson, Y. Pei, D. J. Singh, G. Chen, C.-W. Chu and Z. Ren, *Proc. Natl. Acad. Sci. USA* **2017**, *114*, 10548-10553.

[110] a) J. T. Greenfield, C. D. Unger, M. Chen, N. Izquierdo, K. E. Woo, V. O. Garlea, S. Kamali and K. Kovnir, *Chem. Mater.* **2017**, *29*, 7716-7724; b) J. T. Greenfield, V. Ovidiu Garlea, S. Kamali, M. Chen and K. Kovnir, *J. Solid State Chem.* **2016**, *236*, 222-229; c) D. M. Pajerowski, V. O. Garlea, E. S. Knowles, M. J. Andrus, M. F. Dumont, Y. M. Calm, S. E. Nagler, X. Tong, D. R. Talham and M. W. Meisel, *Phys. Rev. B* **2012**, *86*, 054431.

[111] R. M. Ibberson, *Nucl. Instrum. Methods Phys. Res. A* **2009**, *600*, 47-49.

[112] GEM in *website:* *https://www.isis.stfc.ac.uk/Pages/Gem.aspx*.

[113] Polaris in *website:* *https://www.isis.stfc.ac.uk/Pages/polaris.aspx*.

[114] a) WISH in *website:* https://www.isis.stfc.ac.uk/Pages/Wish.aspx, *Vol*; b) L. C. Chapon, P. Manuel, P. G. Radaelli, C. Benson, L. Perrott, S. Ansell, N. J. Rhodes, D. Raspino, D. Duxbury, E. Spill and J. Norris, *Neutron News* **2011**, *22*, 22-25.

[115] SuperHRPD in *website:* https://www.kek.jp/en/Facility/IMSS/MLF/KENS/BL08/.

[116] SPICA in *website:* https://www.kek.jp/en/Facility/IMSS/MLF/KENS/BL09/.

[117] iMATERIA in *website:* https://j-parc.jp/researcher/MatLife/en/instrumentation/images/BL20.gif.

[118] D1B in *website:* https://www.ill.eu/users/instruments/instruments-list/d1b/description/instrument-layout/.

[119] D2B in *website:* https://www.ill.eu/users/instruments/instruments-list/d2b/description/instrument-layout/.

[120] a) D20 in *website:* https://www.ill.eu/users/instruments/instruments-list/d20/description/instrument-layout/, *Vol*; b) C. H. Thomas, F. H. Paul, E. F. Henry, T. Jacques and C. Pierre, *Meas. Sci. Technol.* **2008**, *19*, 034001.

[121] PSD in *website:* http://www.bnc.hu/?q=node/10, *Vol.*

[122] TOF-ND in *website:* http://www.bnc.hu/?q=node/21.

[123] Echidna in *website:* https://www.ansto.gov.au/user-access/instruments/neutron-scattering-instruments/echidna-high-resolution-powder.

[124] a) Wombat in *website:* https://www.ansto.gov.au/user-access/instruments/neutron-scattering-instruments/wombat-high-intensity-powder-diffractometer; b) A. J. Studer, M. E. Hagen and T. J. Noakes, *Physica B* **2006**, *385-386*, 1013-1015.

[125] a) J.-A. Dolyniuk, J. Wang, M. A. T. Marple, S. Sen, Y. Cheng, A. J. Ramirez-Cuesta and K. Kovnir, *Chem. Mater.* **2018**, *30*, 3419-3428; b) X. Han, H. G. W. Godfrey, L. Briggs,

A. J. Davies, Y. Cheng, L. L. Daemen, A. M. Sheveleva, F. Tuna, E. J. L. McInnes, J. Sun, C. Drathen, M. W. George, A. J. Ramirez-Cuesta, K. M. Thomas, S. Yang and M. Schröder, *Nat. Mater.* **2018**, *17*, 691-696; c) T. Sato, A. J. Ramirez-Cuesta, L. L. Daemen, Y. Cheng and S.-i. Orimo, *Inorg. Chem.* **2018**, *57*, 867-872; d) M. E. Casco, J. Fernández-Catalá, Y. Cheng, L. Daemen, A. J. Ramirez-Cuesta, C. Cuadrado-Collados, J. Silvestre-Albero and E. V. Ramos-Fernandez, *ChemistrySelect* **2017**, *2*, 2750-2753; e) I. Weinrauch, I. Savchenko, D. Denysenko, S. M. Souliou, H. H. Kim, M. Le Tacon, L. L. Daemen, Y. Cheng, A. Mavrandonakis, A. J. Ramirez-Cuesta, D. Volkmer, G. Schütz, M. Hirscher and T. Heine, *Nat. Commun.* **2017**, *8*, 14496; f) M. E. Casco, Y. Q. Cheng, L. L. Daemen, D. Fairen-Jimenez, E. V. Ramos-Fernández, A. J. Ramirez-Cuesta and J. Silvestre-Albero, *Chem. Commun.* **2016**, *52*, 3639-3642; g) P. Yin, B. Wu, E. Mamontov, L. L. Daemen, Y. Cheng, T. Li, S. Seifert, K. Hong, P. V. Bonnesen, J. K. Keum and A. J. Ramirez-Cuesta, *J. Am. Chem. Soc.* **2016**, *138*, 2638-2643; h) T. Sato, A. J. Ramirez-Cuesta, L. Daemen, Y. Q. Cheng, K. Tomiyasu, S. Takagi and S. Orimo, *Chem. Commun.* **2016**, *52*, 11807-11810; i) L. Cai, Y. Shi, K. Hrdina, L. Moore, J. Wu, L. L. Daemen and Y. Cheng, *Phys. Rev. B* **2018**, *97*, 054311; j) Y. Cheng, J. Balachandran, Z. Bi, C. A. Bridges, M. P. Paranthaman, Luke L. Daemen, P. Ganesh and N. Jalarvo, *J. Mater. Chem. A* **2017**, *5*, 15507-15511; k) E. M. Mozur, A. E. Maughan, Y. Cheng, A. Huq, N. Jalarvo, L. L. Daemen and J. R. Neilson, *Chem. Mater.* **2017**, *29*, 10168-10177.

[126] VISION in *website:* *https://neutrons.ornl.gov/vision*.

[127] A. J. Ramirez-Cuesta, *Comput. Phys. Commun.* **2004**, *157*, 226-238.

[128] TOSCA in *website:* *https://www.isis.stfc.ac.uk/Pages/Tosca.aspx*.

[129] NERA in *website:* *http://flnph.jinr.ru/en/facilities/ibr-2/instruments/nera*.

[130] a) G. Ehlers, A. A. Podlesnyak, J. L. Niedziela, E. B. Iverson and P. E. Sokol, *Rev. Sci. Instrum.* **2011**, *82*, 085108; b) G. Ehlers, A. A. Podlesnyak and A. I. Kolesnikov, *Rev. Sci. Instrum.* **2016**, *87*, 093902.

[131] O. Arnold, J. C. Bilheux, J. M. Borreguero, A. Buts, S. I. Campbell, L. Chapon, M. Doucet, N. Draper, R. Ferraz Leal, M. A. Gigg, V. E. Lynch, A. Markvardsen, D. J. Mikkelson, R. L. Mikkelson, R. Miller, K. Palmen, P. Parker, G. Passos, T. G. Perring, P. F. Peterson, S. Ren, M. A. Reuter, A. T. Savici, J. W. Taylor, R. J. Taylor, R. Tolchenov, W. Zhou and J. Zikovsky, *Nucl. Instr. Meth. Phys. Res. A* **2014**, *764*, 156-166.

[132] M. Feng and M. L. Tong, *Chem. Eur. J.* **2018**, *24*, 7574-7594.

[133] IN5 in *website:* *https://www.ill.eu/users/instruments/instruments-list/in5/description/instrument-layout/*.

[134] LET in *website:* *https://www.isis.stfc.ac.uk/Pages/Let.aspx*.

[135] TOFTOF in *website:* . *https://www.mlz-garching.de/toftof*.

[136] NEAT in *website:* *https://www.helmholtz-berlin.de/pubbin/igama_output?modus=einzel&sprache=en&gid=1717&typoid=50722*.

[137] AMATERAS in *website:* *https://j-parc.jp/researcher/MatLife/en/instrumentation/ns_spec.html#bl14*.

[138] PELICAN in *website:* *https://archive.ansto.gov.au/ResearchHub/OurInfrastructure/ACNS/Facilities/Instruments/Pelican/index.htm*.

[139] DCS in *website:* *https://ncnr.nist.gov/instruments/dcs/*.

[140] R. T. Azuah, L. R. Kneller, Y. Qiu, P. L. W. Tregenna-Piggott, C. M. Brown, J. R. D. Copley and R. M. Dimeo, *J. Res. Natl. Inst. Stan. Technol.* **2009**, *114*, 341-358.

[141] C. M. Brown and J. L. Manson, *J. Am. Chem. Soc.* **2002**, *124*, 12600-12605.

[142] W. Zhou, H. Wu, T. J. Udovic, J. J. Rush and T. Yildirim, *J. Phys. Chem. A* **2008**, *112*, 12602-12606.

[143] a) N. Rosenbach, H. Jobic, A. Ghoufi, F. Salles, G. Maurin, S. Bourrelly, P. L. Llewellyn, T. Devic, C. Serre and G. Ferey, *Angew. Chem.* **2008**, *120*, 6713-6717; *Angew. Chem. Int. Ed.* **2008**, *47*, 6611-6615; b) F. Salles, D. I. Kolokolov, H. Jobic, G. Maurin, P. L. Llewellyn, T. Devic, C. Serre and G. Ferey, *J. Phys. Chem. C* **2009**, *113*, 7802-7812; c) F. Salles, S. Bourrelly, H. Jobic, T. Devic, V. Guillerm, P. Llewellyn, C. Serre, G. Ferey and G. Maurin, *J. Phys. Chem. C* **2011**, *115*, 10764-10776; d) D. I. Kolokolov, A. G. Stepanov, V. Guillerm, C. Serre, B. Frick and H. Jobic, *J. Phys. Chem. C* **2012**, *116*, 12131-12136; e) S. Rives, H. Jobic, F. Ragon, T. Devic, C. Serre, G. Ferey, J. Ollivier and G. Maurin, *Microporous Mesoporous Mater.* **2012**, *164*, 259-265; f) S. Rives, H. Jobic, D. I. Kolokolov, A. A. Gabrienko, A. G. Stepanov, Y. Ke, B. Frick, T. Devic, G. Ferey and G. Maurin, *J. Phys. Chem. C* **2013**, *117*, 6293-6302; g) N. A. Ramsahye, J. Gao, H. Jobic, P. L. Llewellyn, Q. Yang, A. D. Wiersum, M. M. Koza, V. Guillerm, C. Serre, C. L. Zhong and G. Maurin, *J. Phys. Chem. C* **2014**, *118*, 27470-27482; h) N. Rosenbach, H. Jobic, A. Ghoufi, T. Devic, M. M. Koza, N. Ramsahye, C. J. Mota, C. Serre and G. Maurin, *J. Phys. Chem. C* **2014**, *118*, 14471-14477.

[144] C. M. Brown, Y. Liu, T. Yildirim, V. K. Peterson and C. J. Kepert, *Nanotechnol.* **2009**, *20*, 204025.

[145] K. Sumida, C. M. Brown, Z. R. Herm, S. Chavan, S. Bordiga and J. R. Long, *Chem. Commun.* **2011**, *47*, 1157-1159.

[146] S. Miyatsu, M. Kofu, A. Nagoe, T. Yamada, M. Sadakiyo, T. Yamada, H. Kitagawa, M. Tyagi, V. García Sakai and O. Yamamuro, *Phys. Chem. Chem. Phys.* **2014**, *16*, 17295-17304.

[147] a) R. Caciuffo, T. Guidi, G. Amoretti, S. Carretta, N. Magnani, P. Santini and C. Mondelli, *Physica B* **2006**, *385-386*, 301-306; b) G. Amoretti, R. Caciuffo, S. Carretta, T. Guidi, N. Magnani and P. Santini, *Inorg. Chim. Acta* **2008**, *361*, 3771-3776; c) S. Carretta, P. Santini, G. Amoretti, T. Guidi, J. R. D. Copley, Y. Qiu, R. Caciuffo, G. Timco and R. E. P. Winpenny, *Phys. Rev. Lett.* **2007**, *98*, 167401.

[148] a) A. Zheludev, Z. Honda, C. L. Broholm, K. Katsumata, S. M. Shapiro, A. Kolezhuk, S. Park and Y. Qiu, *Phys. Rev. B* **2003**, *68*, 134438; b) T. Masuda, A. Zheludev, H. Manaka, L. P. Regnault, J. H. Chung and Y. Qiu, *Phys. Rev. Lett.* **2006**, *96*, 047210; c) K. Matan, D. Grohol, D. G. Nocera, T. Yildirim, A. B. Harris, S. H. Lee, S. E. Nagler and Y. S. Lee, *Phys. Rev. Lett.* **2006**, *96*, 247201; d) T. Hong, M. Kenzelmann, M. M. Turnbull, C. P. Landee, B. D. Lewis, K. P. Schmidt, G. S. Uhrig, Y. Qiu, C. Broholm and D. Reich, *Phys. Rev. B* **2006**, *74*, 094434; e) J. S. Helton, K. Matan, M. P. Shores, E. A. Nytko, B. M. Bartlett, Y. Yoshida, Y. Takano, A. Suslov, Y. Qiu, J. H. Chung, D. G. Nocera and Y. S. Lee, *Phys. Rev. Lett.* **2007**, *98*, 107204; f) S. H. Lee, H. Kikuchi, Y. Qiu, B. Lake, Q. Huang, K. Habicht and K. Kiefer, *Nat. Mater.* **2007**, *6*, 853; g) A. Zheludev, V. O. Garlea, T. Masuda, H. Manaka, L. P. Regnault, E. Ressouche, B. Grenier, J. H. Chung, Y. Qiu, K. Habicht, K. Kiefer and M. Boehm, *Phys. Rev. B* **2007**, *76*, 054450; h) V. O. Garlea, A. Zheludev, L. P. Regnault, J. H. Chung, Y. Qiu, M. Boehm, K. Habicht and M. Meissner, *Phys. Rev. Lett.* **2008**, *100*, 037206; i) J. H. Kim, S. Ji, S. H. Lee, B. Lake, T. Yildirim, H. Nojiri, H. Kikuchi, K. Habicht, Y. Qiu and K. Kiefer, *Phys. Rev. Lett.* **2008**,

101, 107201; j) A. T. Savici, G. E. Granroth, C. L. Broholm, D. M. Pajerowski, C. M. Brown, D. R. Talham, M. W. Meisel, K. P. Schmidt, G. S. Uhrig and S. E. Nagler, *Phys. Rev. B* **2009**, *80*, 094411; k) J. Brambleby, J. L. Manson, P. A. Goddard, M. B. Stone, R. D. Johnson, P. Manuel, J. A. Villa, C. M. Brown, H. Lu, S. Chikara, V. Zapf, S. H. Lapidus, R. Scatena, P. Macchi, Y.-s. Chen, L.-C. Wu and J. Singleton, *Phys. Rev. B* **2017**, *95*, 134435; l) J. L. Manson, T. Lancaster, S. J. Blundell, Y. Qiu, J. Singleton, P. Sengupta, F. L. Pratt, J. Kang, C. Lee and M.-H. Whangbo, *Polyhedron* **2010**, *29*, 514-520; m) T. Hong, C. Stock, I. Cabrera, C. Broholm, Y. Qiu, J. B. Leao, S. J. Poulton and J. R. D. Copley, *Phys. Rev. B* **2010**, *82*, 184424.

[149] M. Kenzelmann, Y. Chen, C. Broholm, D. H. Reich and Y. Qiu, *Phys. Rev. Lett.* **2004**, *93*, 017204.

[150] M. Hälg, D. Hüvonen, N. P. Butch, F. Demmel and A. Zheludev, *Phys. Rev. B* **2015**, *92*, 104416.

[151] a) G. E. Granroth, A. I. Kolesnikov, T. E. Sherline, J. P. Clancy, K. A. Ross, J. P. C. Ruff, B. D. Gaulin and S. E. Nagler, *J. Phys. Conf. Ser.* **2010**, *251*, 012058; b) M. B. Stone, J. L. Niedziela, D. L. Abernathy, L. DeBeer-Schmitt, G. Ehlers, O. Garlea, G. E. Granroth, M. Graves-Brook, A. I. Kolesnikov, A. Podlesnyak and B. Winn, *Rev. Sci. Instrum.* **2014**, *85*, 045113.

[152] a) H.-W. Wang, M. J. DelloStritto, N. Kumar, A. I. Kolesnikov, P. R. C. Kent, J. D. Kubicki, D. J. Wesolowski and J. O. Sofo, *J. Phys. Chem. C* **2014**, *118*, 10805-10813; b) S. H. Overbury, A. I. Kolesnikov, G. M. Brown, Z. Zhang, G. S. Nair, R. L. Sacci, R. Lotfi, A. C. T. van Duin and M. Naguib, *J. Am. Chem. Soc.* **2018**, *140*, 10305-10314.

[153] a) A. I. Kolesnikov, A. Podlesnyak, R. A. Sadykov, V. E. Antonov, M. A. Kuzovnikov, G. Ehlers and G. E. Granroth, *Phys. Rev. B* **2016**, *94*, 134301; b) A. I. Kolesnikov, G. F. Reiter, N. Choudhury, T. R. Prisk, E. Mamontov, A. Podlesnyak, G. Ehlers, A. G. Seel, D. J. Wesolowski and L. M. Anovitz, *Phys. Rev. Lett.* **2016**, *116*, 167802.

[154] J. Gaudet, A. M. Hallas, A. I. Kolesnikov and B. D. Gaulin, *Phys. Rev. B* **2018**, *97*, 024415.

[155] a) A. Podlesnyak, L. M. Anovitz, A. I. Kolesnikov, M. Matsuda, T. R. Prisk, S. Toth and G. Ehlers, *Phys. Rev. B* **2016**, *93*, 064426; b) K. W. Plumb, K. Hwang, Y. Qiu, L. W. Harriger, G. E. Granroth, Alexander I. Kolesnikov, G. J. Shu, F. C. Chou, C. Rüegg, Y. B. Kim and Y.-J. Kim, *Nat. Phys.* **2015**, *12*, 224.

[156] ARCS in *website:* *https://neutrons.ornl.gov/arcs*.

[157] HYSPEC in *website:* *https://neutrons.ornl.gov/hyspec*.

[158] MERLIN in *website:* *https://www.isis.stfc.ac.uk/Pages/Merlin.aspx*.

[159] MAPS in *website:* *https://www.isis.stfc.ac.uk/Pages/MAPS.aspx*.

[160] MARI in *website:* *https://www.isis.stfc.ac.uk/Pages/MARI.aspx*.

[161] 4SEASONS in *website:* *https://j-parc.jp/researcher/MatLife/en/instrumentation/images/4seasons.pdf*.

[162] C. B. Fu, T. R. Gentile, G. L. Jones, W. C. Chen, R. Erwin, S. Watson, C. Broholm, J. A. Rodriguez-Rivera and J. Scherschligt, *Physica B* **2011**, *406*, 2419-2423.

[163] T. Hong, K. P. Schmidt, K. Coester, F. F. Awwadi, M. M. Turnbull, Y. Qiu, J. A. Rodriguez-Rivera, M. Zhu, X. Ke, C. P. Aoyama, Y. Takano, H. Cao, W. Tian, J. Ma, R. Custelcean, H. D. Zhou and M. Matsuda, *Phys. Rev. B* **2014**, *89*, 174432.

[164] T. Hong, Y. Qiu, M. Matsumoto, D. A. Tennant, K. Coester, K. P. Schmidt, F. F. Awwadi, M. M. Turnbull, H. Agrawal and A. L. Chernyshev, *Nat. Commun.* **2017**, *8*, 15148.

[165] T. Hong, M. Matsumoto, Y. Qiu, W. Chen, T. R. Gentile, S. Watson, F. F. Awwadi, M. M. Turnbull, S. E. Dissanayake, H. Agrawal, R. Toft-Petersen, B. Klemke, K. Coester, K. P. Schmidt and D. A. Tennant, *Nat. Phys.* **2017**, *13*, 638.

[166] E. Mamontov and K. W. Herwig, *Rev. Sci. Instrum.* **2011**, *82*, 085109.

[167] Z. Wang, L. L. Daemen, Y. Cheng, E. Mamontov, P. V. Bonnesen, K. Hong, A. J. Ramirez-Cuesta and P. Yin, *Chem. Eur. J.* **2016**, *22*, 14131-14136.

[168] IN16B in *website:* *https://www.ill.eu/users/instruments/instruments-list/in16b/description/instrument-layout/*.

[169] IRIS in *website:* *https://www.isis.stfc.ac.uk/Pages/iris.aspx*.

[170] OSIRIS in *website:* *https://www.isis.stfc.ac.uk/Pages/osiris.aspx*.

[171] SPHERES in *website:* *https://www.mlz-garching.de/spheres*.

[172] DNA in *website:* *https://j-parc.jp/researcher/MatLife/en/instrumentation/images/DNA.pdf*.

[173] EMU in *website:* *http://www.ansto.gov.au/ResearchHub/OurInfrastructure/ACNS/Facilities/Instruments/Emu/index.htm*.